Published by Institute of Physics Publishing for SISSA

Received: *November 9, 2004*
Revised: *February 25, 2005*
Accepted: *April 12, 2005*
Published: *April 26, 2005*

On charged black holes in anti-de Sitter space

Dominic Brecher,[a] Jianyang He[a] and Moshe Rozali[ab]

[a] *Department of Physics and Astronomy, University of British Columbia Vancouver, British Columbia V6T 1Z1, Canada*
[b] *Kavli Institute for Theoretical Physics, University of California Santa Barbara, CA 93106-4030, U.S.A.*
E-mail: brecher@physics.ubc.ca, jyhe@physics.ubc.ca, rozali@physics.ubc.ca

Abstract: We study the region inside the event horizon of charged black holes in five dimensional asymptotically anti-de Sitter space, using as a probe two-sided correlators which are dominated by spacelike geodesics penetrating the horizon. The spacetimes we investigate include the Reissner-Nordström black hole and perturbations thereof. The perturbed spacetimes can be found exactly, enabling us to perform a local scan of the region between the inner and outer horizons. Surprisingly, the two-sided correlators we calculate seem to be geometrically protected from the instability of the inner horizon.

Keywords: AdS-CFT and dS-CFT Correspondence, Black Holes in String Theory.

Contents

1. Introduction and summary

Generic black holes, those with non-zero charge and/or angular momentum, have a causal structure very different to that of the more familiar Schwarzschild black hole. This is a source of new and interesting phenomena. In addition to the outer event horizon, the geometry contains an inner horizon surrounding a singularity, which is timelike. This inner horizon is also a Cauchy horizon — it bounds a region outside of the Cauchy development of an initial data set. Finally, the inner horizon is a surface of infinite blue shift — analysis at the linearised level shows that an arbitrary perturbation gets magnified by the geometry near that surface [1]–[3].

It is then generally expected that the inner horizon is unstable to small perturbations, which back-react strongly on the geometry, likely resulting in a singularity. The spacetime effectively ends at or before one reaches the Cauchy horizon, and so the cosmic censorship conjecture [4] is upheld. However, the precise mechanism for this expected instability, and the resulting spacetime structure, have not yet been settled. For recent efforts towards clarifying this issue within classical general relativity see [5], and for a recent investigation of three dimensional rotating black holes in this context see [6].

This set of issues could be studied within the AdS/CFT correspondence [7, 8] although, as for other interesting phenomena[1] associated with black holes, to study the physics one would have to probe the geometry behind an event horizon. Early efforts to do that are [10]-[13]. Here, we will use the set of ideas introduced in [14] and further developed in [6] and [15]–[20]. Namely, we will study a set of observables which depend in a precise sense on the physics behind the horizon.[2]

The observables are correlation functions of operators which are inserted on the two disconnected boundaries of the eternal black hole spacetime [14]. These are the objects we will use to probe the above questions associated with generic black holes. In the limit of large operator dimension, the correlators are approximated by the contribution from a single spacelike geodesic, which penetrates the event horizon. For a precise explanation of this approximation we refer the reader to [14, 17].

This is an explicit realisation of work by Israel [22], in which parallels were drawn between the concepts of the thermofield formalism of field theory (see, e.g., [23] for a review) and black hole physics. The fictitious Hilbert space in the thermofield formalism is just the space of states behind the event horizon of the eternal black hole. By tracing over the fictitious states, we recover the thermal behaviour of the physical states. In the AdS version, correlators of operators inserted on a single boundary will be ordinary thermal correlation functions, but one may also consider correlation functions of operators inserted on two opposite boundaries. As explained in [14, 17], one can compute such correlators from those of operators inserted on a single boundary, by analytic continuation, simply shifting the argument of one operator by half a period of imaginary time.

The outline of the paper, and a summary of results is as follows.

We begin, in section 2, by introducing the five dimensional AdS-Reissner-Nordström (AdS-RN) geometry, following [24]. We discuss coordinate systems and complexification of the metric, and draw the Penrose diagram which encodes the causal structure. We should note that we will only be concerned with the non-extreme black hole, since the extreme solution has only one asymptotic region, so there are simply no such objects as two-sided correlators. This makes sense, since the extreme black hole is at zero temperature [24].

In sections 3 and 4, we investigate correlation functions of neutral and charged operators respectively. As a preparation for the perturbed case we are interested in their late time behaviour. We give arguments that, at least for part of the black hole parameter space — for near-extreme black holes — such late time correlators are dominated by real geodesics, unlike the situation for the AdS-Schwarzschild black hole [17]. The discussion in this case does not involve the subtleties of [17], as there is no branch cut or singularity in the correlators. On the other hand, for black holes sufficiently far from extremality (or sufficiently close to being small and neutral black holes) various properties become qualitatively similar to the Schwarzschild case. In those cases we expect the real geodesics do not dominate the correlators at late times.

[1]See, however, recent efforts to construct naked singularities in asymptotically AdS spaces [9].

[2]Though, in the spirit of black hole complementarity [21], should also be recoverable from observations outside the horizon only.

JHEP04(2005)004

As emphasised in [18], it seems that the field theory only encodes the region of spacetime within the Cauchy horizon. In that sense, the AdS/CFT correspondence would uphold the cosmic censorship conjecture, at least for the observables we consider. It would be interesting to see if this is a more general feature of the field theory.

In section 5 we turn to an analysis of a perturbed AdS-RN spacetime. For perturbations which move at the speed of light (ingoing or outgoing only), one can use the methods of Poisson and Israel [25] to find the perturbed metric exactly. By varying the time at which the metric is perturbed, one can perform a scan of (at least some part of) the region between the inner and outer horizons,[3] again using the two-sided correlators as a probe. We demonstrate this through the simplest example of an infinitely thin perturbation, an outgoing thin shell of null matter.

We confine ourselves here to calculating the dependence of the correlators on the time at which the perturbation leaves the boundary. This demonstrates that the gauge theory is sensitive to a perturbation of spacetime which is localised purely behind the outer horizon. It would be interesting to read off from these correlators the dramatic behaviour expected when mass inflation [25] sets in. We leave this to future work [26], but we comment that so far it seems that our correlators are screened from this catastrophic instability by some subtle geometrical effects, which we explain below.

2. Classical geometry

In this section we discuss the classical geometry of the electrically charged AdS-RN black hole, its complexification and causal structure. We restrict attention to aspects of the geometry which are relevant for us, more details can be found in [24].

The spacetime. The five dimensional solution[4] takes the form [24]

$$\mathrm{d}s^2 = -f(r)\mathrm{d}t^2 + \frac{\mathrm{d}r^2}{f(r)} + r^2\mathrm{d}\Omega_3^2\,, \qquad A = \left(-\frac{1}{c}\frac{Q}{r^2} + \Phi\right)\mathrm{d}t\,, \tag{2.1}$$

where

$$f(r) = 1 + \frac{r^2}{l^2} - \frac{M}{r^2} + \frac{Q^2}{r^4} \equiv \frac{\Delta(r)}{l^2 r^4}\,, \qquad \Delta(r) = r^6 + l^2 r^4 - l^2 M r^2 + l^2 Q^2\,, \tag{2.2}$$

$c = 2/\sqrt{3}$, Φ is a constant and M and Q are respectively proportional to the mass and charge of the black hole. The spacetime is asymptotically AdS, with curvature radius l, the boundary theory living on $\mathbb{R} \times S^3$. From now on, we will take $l = 1$. The boundary is at $r = \infty$ and there is a timelike singularity at $r = 0$.

Horizons of the metric are given by the real positive roots of $\Delta(r)$. We will often work with the variable $x = r^2$, $\Delta(x)$ being a cubic in x. Since, with $M > 0$,

$$\Delta(0) = Q^2 > 0 \qquad \text{and} \qquad \frac{\mathrm{d}\Delta}{\mathrm{d}x}(0) = -M < 0\,, \tag{2.3}$$

[3]This is somewhat similar to the discussion in [19], though here the perturbed metric is on-shell.

[4]A solution of five dimensional Einstein-Maxwell theory with a negative cosmological constant. The ten dimensional origins are discussed in [24].

one root of Δ must occur for $x < 0$. We denote this negative root by $-x_0 = -r_0^2$. There are then at most two positive real roots, denoted by $x_\pm = r_\pm^2$, with $x_+ \geq x_-$. We will thus write

$$\Delta(x) = (x + x_0)(x - x_-)(x - x_+)\,. \tag{2.4}$$

It is easy to show that $x_0 = 1 + x_- + x_+$, so we will only need to specify $x_\pm$. The non-extreme black hole, with $x_+ > x_-$, has an outer event horizon at r_+ and an inner Cauchy horizon at r_-. The extreme solution, with $x_+ = x_-$, has a single event horizon at r_+.

The surface gravities at the outer and inner horizons are, respectively,

$$\kappa_\pm = \frac{(x_0 + x_\pm)(x_+ - x_-)}{x_\pm^{3/2}}\,, \tag{2.5}$$

the temperature of the black hole being $T = \kappa_+/(2\pi) = 1/\beta$. The dual field theory is thus in a thermal state at temperature T. One can then work [24] with either fixed charge (the canonical ensemble) or fixed potential (the grand canonical ensemble). In the latter case, the electrostatic potential in the field theory is given by the constant Φ, which can be fixed as $\Phi = (1/c)(Q/x_+)$ such that $A_t(r_+) = 0$. In terms of the bulk physics, Φ is the electrostatic potential difference between the horizon and infinity.

Embedding into the complex plane. There are six distinct regions of the spacetime, the Penrose diagram consisting of an infinite sequence of these basic blocks. As was emphasized in [18], and as will be discussed below, the region behind the inner horizon does not seem to play any role in the field theory, therefore we can restrict attention to one copy of these basic blocks.

To describe the global structure, one can pass to Kruskal-like coordinates to describe the maximal analytic extension of the space. Alternatively, as in [6] and [16]–[18], one can use different Schwarzschild coordinate patches to describe the global extension. They are embedded into complex Schwarzschild time, with $t = t_L + it_E$ having a constant imaginary part in each patch. This is shown in figure 1, in which we define $t_E = 0$ in the right asymptotic region. Then, as in [17], crossing the event horizon at r_+ shifts t_E by $\pi/(2\kappa_+) = i\beta/4$ so, to move from a point on the right-hand boundary to the symmetric point on the left-hand boundary, we shift $t \to -(t + i\beta/2)$. Crossing the Cauchy horizon at r_- instead would shift t_E by $\pi/(2\kappa_-)$ although this will not be relevant to the boundary field theory.[5]

The Penrose diagram. The basic features of the Penrose diagram are shown by the behaviour of radial null geodesics. As in the uncharged case [17], the boundaries and the singularities cannot both be drawn as straight lines. For radial null geodesics, we work with the lagrangian

$$\mathcal{L} = -f(r)\dot{t}^2 + \frac{\dot{r}^2}{f(r)} = 0\,, \tag{2.6}$$

[5]The embedding into complex time can be repeated infinitely in both directions, by shifting t_E appropriately, as one crosses each horizon.

JHEP04(2005)004

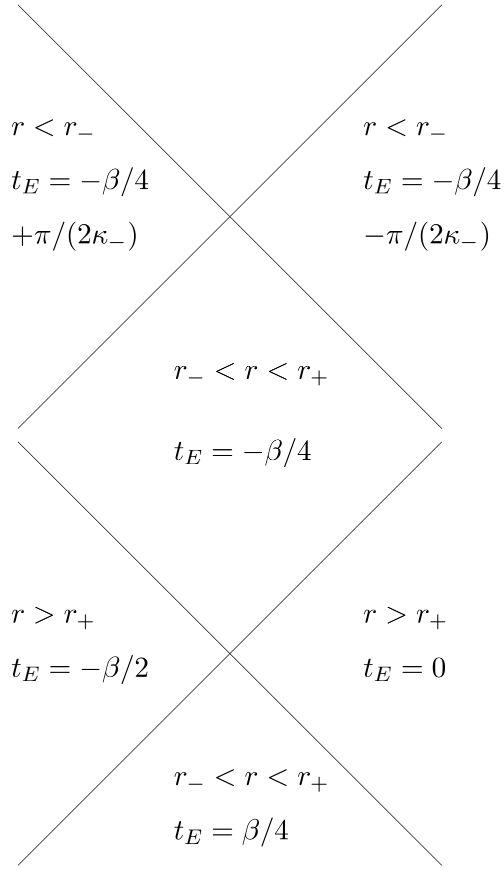

Figure 1: The embedding into complex Schwarzschild time, showing the constant imaginary parts of $t = t_L + it_E$.

where dots denote differentiation with respect to the affine parameter λ. There is a conserved energy, E, associated with the Killing vector $\partial/\partial t$, in terms of which the geodesic equations become

$$\dot{t} = \frac{E}{f(r)}, \qquad \dot{r}^2 = E^2 . \tag{2.7}$$

For ingoing geodesics which start at the boundary $r = \infty$ at $t = 0$, the time t as a function of r is given by

$$t(r) = \int_r^\infty \frac{\mathrm{d}r'}{f(r')} = \int_{r^2}^\infty \frac{\mathrm{d}x}{2} \frac{x^{3/2}}{(x+x_0)(x-x_-)(x-x_+)} . \tag{2.8}$$

Explicitly, for $r < r_-$,

$$\begin{aligned} t(r) = & -\frac{x_0^{3/2}}{(x_0+x_-)(x_0+x_+)}\left(\tan^{-1}\left(\frac{r}{r_0}\right) - \frac{\pi}{2}\right) - \frac{1}{\kappa_-}\tanh^{-1}\left(\frac{r}{r_-}\right) + \\ & + \frac{1}{\kappa_+}\tanh^{-1}\left(\frac{r}{r_+}\right) - \frac{i\pi}{2}\left(\frac{1}{\kappa_+} - \frac{1}{\kappa_-}\right), \end{aligned} \tag{2.9}$$

where the pure imaginary terms arise from integrating over the two poles at $x = x_\pm$. These are just the shifts in t_E discussed above. Such a geodesic will reach the singularity $r = 0$ at a finite time

$$t_{\rm sing} = \frac{\pi}{2} \frac{x_0^{3/2}}{(x_0 + x_-)(x_0 + x_+)} - \frac{i\pi}{2} \left(\frac{1}{\kappa_+} - \frac{1}{\kappa_-} \right) \tag{2.10}$$

whose real part is positive. Conversely, a geodesic which hits the singularity at $t_L = 0$, must leave the boundary at time

$$t_c = -\frac{\pi}{2} \frac{x_0^{3/2}}{(x_0 + x_-)(x_0 + x_+)} < 0\,, \tag{2.11}$$

from which we conclude that one cannot draw both the boundaries and the singularities as straight lines in the Penrose diagram. Choosing the boundaries to be straight lines, then the singularities must be *bowed out*, the situation demonstrated in figure 2. However, it will become clear that this behaviour has no influence on the boundary theory. In particular the critical value t_c in the Schwarzschild case of [17] plays no role in the discussion of correlation functions here.

Kruskal coordinates. As in the asymptotically flat case [27], we need two Kruskal-like coordinates patches to cover the region $0 < r < \infty$, one being valid through the outer horizon, the other being valid through the inner horizon. In the usual way, we first define the tortoise coordinate

$$r_* = \int_0^r \frac{\mathrm{d}r'}{f(r')} + C = x_0' \tan^{-1}\left(\frac{r}{r_0}\right) + \frac{1}{2\kappa_+} \ln\left(\frac{r - r_+}{r + r_+}\right) - \frac{1}{2\kappa_-} \ln\left(\frac{r - r_-}{r + r_-}\right), \tag{2.12}$$

where $x_0' = x_0^{3/2}/((x_0 + x_+)(x_0 + x_-))$ and we have chosen the constant C so as to make r_* real for $r > r_+$. As we cross the horizons from this region, we pick up the same constant imaginary terms as in the expression (2.9) for t, giving an embedding of the spacetime into the complex coordinate plane.

To cover the entire range of r, define the light cone coordinates $u = t - r_*, v = t + r_*$. For $r > r_-$, transform according to

$$U^+ = -e^{-\kappa_+ u} = T^+ - X^+\,, \qquad V^+ = e^{+\kappa_+ v} = T^+ + X^+ \tag{2.13}$$

whereas for $r < r_+$, take

$$U^- = -e^{+\kappa_- u} = T^+ - X^+\,, \qquad V^- = e^{-\kappa_- v} = T^- + X^-\,. \tag{2.14}$$

The outer horizon is given by $T^{+2} - X^{+2} = 0$ and the inner has $T^{-2} - X^{-2} = 0$. The metric becomes

$$\mathrm{d}s^2 = \frac{1}{\kappa_\pm^2} f(r)\, e^{\mp 2\kappa_\pm r_*} (-(\mathrm{d}T^\pm)^2 + (\mathrm{d}X^\pm)^2)\,, \tag{2.15}$$

where for $r > r_-$, $r(T^+, X^+)$ is determined implicitly by

$$T^{+2} - X^{+2} = -e^{2\kappa_+ r_*} = -e^{2\kappa_+ x_0' \tan^{-1}(r/r_0)} \left(\frac{r - r_+}{r + r_+}\right) \left(\frac{r + r_-}{r - r_-}\right)^{\kappa_+/\kappa_-} \tag{2.16}$$

JHEP04(2005)004

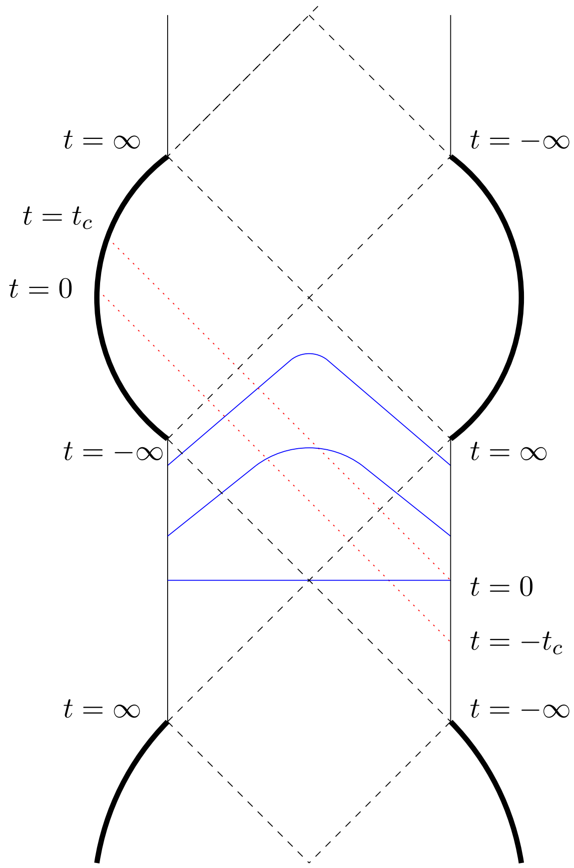

Figure 2: The Penrose diagram repeats itself in both directions. Radial null geodesics are dotted red, radial spacelike geodesics are solid blue, the inner and outer horizons are dashed and the singularities are bold. We have chosen to draw the boundaries as vertical lines, in which case the singularities are bowed out. The values of t all denote those of t_L, the real part of complex time.

and for $r<r_+$, $r(T^-,X^-)$ is determined by

$$T^{-2}-X^{-2}=-e^{-2\kappa_- r_*}=-e^{-2\kappa_- x_0' \tan^{-1}(r/r_0)}\left(\frac{r_++r}{r_+-r}\right)^{\kappa_-/\kappa_+}\left(\frac{r_--r}{r_-+r}\right). \tag{2.17}$$

However, the boundaries and singularities are covered by different coordinate patches, which makes comparison of them impossible.

One can instead follow [27] and use the coordinates defined in (2.13) for the regions $r>r_+$ *and* $r<r_-$. In the region $r_-<r<r_+$, we instead define the light cone coordinates $u=t+r_*, v=-(t-r_*)$ and use

$$U=e^{\kappa_+ u}=T-X\,, \qquad V=e^{\kappa_+ v}=T+X\,. \tag{2.18}$$

The metric can be written everywhere as

$$\mathrm{d}s^2=\frac{|f(r)|}{\kappa_+^2}e^{-2\kappa_+ r_*}(-\mathrm{d}T^2+\mathrm{d}X^2) \tag{2.19}$$

which is analytic except at the inner horizon $r = r_-$. The radial coordinate r is determined implicitly by

$$T^2 - X^2 = \mp e^{2\kappa_+ x_0' \tan^{-1}(r/r_0)} \left(\frac{|r - r_+|}{r + r_+}\right) \left(\frac{r + r_-}{|r - r_-|}\right)^{\kappa_+/\kappa_-} \tag{2.20}$$

the $\mp$ sign corresponding to the regions $r > r_+$ and $r < r_-$, and $r_- < r < r_+$, respectively.

Now we can compare the boundaries and singularities in the first set of coordinates. In the limits

$$\begin{aligned} r \to \infty \qquad &\Rightarrow \qquad T^2 - X^2 \to -e^{\pi\kappa_+ x_0'} < -1\,, \\ r \to 0 \qquad &\Rightarrow \qquad T^2 - X^2 \to -1 \end{aligned} \tag{2.21}$$

so in a (T, X) spacetime diagram, the hyperboli representing the singularities will be further away from the origin than the hyperboli representing the boundaries. This is opposite to the Schwarzschild case [17]. Following those arguments, one sees that on the resulting Penrose diagram if we draw the singularity $r = 0$ as a vertical line, the boundary $r = \infty$ must be bowed out. Alternatively, we can use a conformal transformation to make the singularity bowed out while keeping the boundary vertical. The latter case is shown schematically in figure 2. (In this case, to bring the boundaries of the spacetime to a finite coordinate distance we can, for example, let $U = e^{\pi\kappa_+ x_0'/2} \tan \tilde{u}$ and $V = e^{\pi\kappa_+ x_0'/2} \tan \tilde{v}$.)

3. Neutral correlation functions

We now discuss features of correlation functions of operators which are electrically neutral. When we put insertions on both boundaries, the correlation functions are dominated (in the limit of high dimensional operators) by spacelike geodesics, as was explained in [14]. Such geodesics are only sensitive to the metric, and not to the background electric field. In the present section, we can restrict ourselves to symmetric geodesics (which reach the boundaries at the same value of $t_L = t_0$), since all others can be obtained by time translation.

It is instructive to compare our discussion to that of the neutral black hole in [17]. The geometry in that case contains a singularity, which results in a specific feature of the geodesics – the regularised length goes to $-\infty$ at finite boundary time, and therefore the corresponding correlator diverges. This is incompatible with the structure of field theory correlation functions, which can be shown to be bounded (by their values at $t_L = 0$). Luckily, one can also show by analysis of the Euclidean slice of the geometry that at $t_L = 0$ the correlators are dominated by complex geodesics, and the real geodesic is subdominant. It is therefore plausible that for any value of t_L the correlator is given by the same linear combination of the complex geodesics, thus avoiding the contradiction. The signature of the bulk singularity is then seen in an appropriate analytic continuation of the field theory results.

The two motivations for that conclusion are absent for near-extreme black holes. First, and for all black hole parameters, the region of our geometry which is probed by the geodesics is non-singular, and so the regularised length of the real geodesic behaves more sensibly — we will see that it is finite for any finite time, and goes to $+\infty$ at late boundary times, corresponding to a sensible exponential decay of the correlators at late time.

Secondly, for the near-extreme black holes, it will become clear that the correlators are bounded by their values at $t_L = 0$. The proper length of the relevant geodesic is a monotonically increasing function of energy, with minimum value at $E = 0$ (corresponding to $t_L = 0$). This is not the case for black holes far from extremality, however, and in that case we would expect the same subtleties of [17].

Finally, analysis of the Euclidean slice of the geometry reveals that for near-extreme black holes, the real geodesic dominates any complex ones, if such geodesics exist. It is then plausible that this real geodesic dominates the correlator at any t_L, in particular for late boundary time, setting the stage to use these geodesics to probe the structure of the perturbed spacetime.

We start in subsection 3.1 by discussing the qualitative features of the real geodesics, before presenting a more quantitative calculation of the correlation functions. As in the null case above, the geodesics are specified by the value of the energy E. In subsection 3.3, we turn to discussing in detail the relation between E and the boundary time, $t(E)$, and in subsection 3.4 we compute the length of the geodesics, which will determine the correlators in our approximation. We discuss the euclidean slice of the geometry in subsection 3.4, showing that for appropriate black hole parameters the real geodesic dominates the correlation functions.

3.1 Qualitative features

Radial spacelike geodesics. For radial spacelike geodesics, and normalizing appropriately, the lagrangian is

$$\mathcal{L} = -f(r)\dot{t}^2 + \frac{\dot{r}^2}{f(r)} = 1\,. \tag{3.1}$$

The geodesic equations are

$$\dot{t} = \frac{E}{f(r)}\,, \qquad \dot{r}^2 = E^2 + f(r) \equiv E^2 - V(r)\,, \tag{3.2}$$

the latter describing a particle of unit mass and of energy E^2 moving in an effective potential $V(r) = -f(r)$. General properties of the geodesics[6] can thus be read off from figure 3, in which the effective potential is shown.

The extreme case is relatively uninteresting since there is no region between the horizon and the singularity which geodesics can probe. Geodesics with $E^2 > 0$ fall all the way into the singularity; those with $E^2 = 0$ reach the single event horizon before returning to the (same) boundary.

The non-extreme case has the following qualitative features:

[6]The uncharged, non-rotating geodesics discussed here resemble geodesics in the AdS-Schwarzschild geometry which carry angular momentum [17].

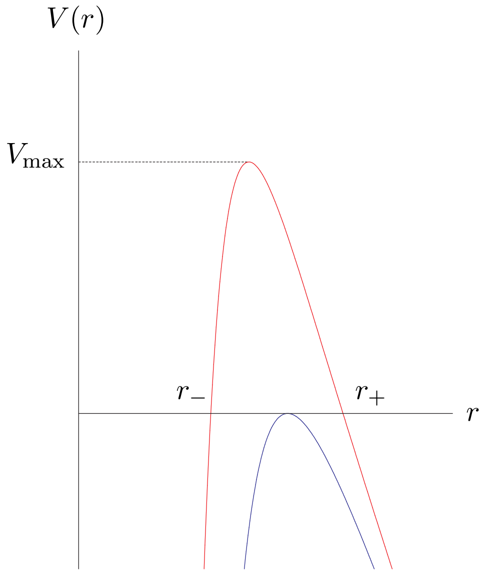

Figure 3: The effective potential in the non-extreme case is shown in red, and the extreme case in blue.

- All geodesics with $E^2 \leq V_{\max}$ return to the asymptotic region $r = \infty$, so will connect the two boundaries. The endpoints lie on the two opposite boundaries, as can be seen by inspecting $t(\lambda)$.

- Geodesics with $0 < E^2 \leq V_{\max}$ will penetrate the outer horizon, and reach some minimal turning point between the two horizons. They cannot penetrate the inner horizon, and will in fact accumulate at some finite distance from it (the radius for which the potential attains its maximum $V_{\max}$), as $E^2 \to V_{\max}$.

- Geodesics with $E = V_{\max}$ penetrate the furthest before returning to the boundary. These geodesics will turn out to have diverging boundary times.

- Geodesics with $E^2 > V_{\max}$ will fall into the singularity, where our approximation breaks down. As the boundary time diverges before we reach this range of E^2, it seems that such trajectories do not contribute to any gauge theory process.

Apparently, at least for the observables we are interested in, the region beyond the Cauchy horizon is not encoded in the gauge theory. Similar conclusions about three dimensional rotating black holes have been obtained in [18]. Moreover, the geodesics do not even reach the Cauchy horizon itself, reaching at most some minimal distance[7] from it. We will see later that, even when perturbing the spacetime, the observables of interest are screened from any dramatic behaviour associated with the Cauchy horizon by this geometrical effect.

[7]This minimal distance can be large for far from extreme black holes, and goes to zero in the extreme limit.

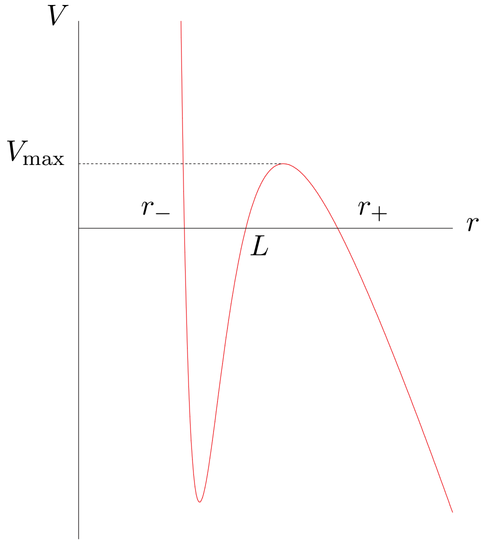

Figure 4: The effective potential for a rotating geodesic with $x_- < L^2 < x_+$. Other choices of the relative magnitude of L^2, x_- and x_+ simply switch the roots. If L^2 is equal to either x_- or x_+, then those two roots will coalesce. The local maximum $V_{\max}$ is also shown.

Rotating spacelike geodesics. Let us add an angular momentum L, conjugate to the azimuthal angle ϕ on the boundary three-sphere.[8] It is the conserved quantity associated with the Killing vector $\partial/\partial\phi$, the relevant geodesic equation being

$$\dot{\phi} = \frac{L}{r^2}\,. \tag{3.3}$$

In this case, the effective potential is modified to $V(r) = -f(r)(1 - L^2/r^2)$ which, in addition to r_+ and r_-, has an additional root at $r = |L|$. A sketch of one possibility is given in figure 4.

In the vicinity of the singularity at $r = 0$, the potential is very different to the non-rotating case: for an arbitrarily small angular momentum, it turns around at small values of r. Consequently, for sufficiently large E one can come arbitrarily close to the singularity and still return to the asymptotic region $r = \infty$; naively the corresponding two-sided correlators are sensitive to the region inside the inner horizon.

However, a closer inspection reveals that such geodesics are irrelevant for the two-sided correlators. Once again, as $E^2 \to V_{\max}$, the boundary time diverges. In addition, the behaviour of $t(\lambda)$ shows that these geodesics connect two boundary points on the *same* side of the Penrose diagram. It is not clear what role, if any, such components play in the field theory dual, since inner horizon instabilities are likely to change the causal structure and eliminate these additional boundaries.

The qualitative details of the rotating trajectories with $E^2 \leq V_{\max}$ depend only on the relative values of r_+ and L. For $|L| > r_+$ the geodesics do not penetrate the outer horizon, making them uninteresting for our purposes. On the other hand, for $|L| < r_+$ the situation

[8]For more general rotation, one replaces L^2 by the relevant Casimir operator.

JHEP04(2005)004

is basically unchanged from the non-rotating case, the geodesics for which $0 < E^2 \leq V_{\max}$ being relevant to us.

3.2 Boundary time

In this subsection we describe the relation between (the real part of) the boundary time t_0 and the energy E. We are interested in symmetric geodesics which start at a point t_0 on the boundary, and end at the point $-(t_0 + i\beta/2)$ on the other boundary. Taking r_E to denote the turning point for a trajectory of energy E^2, we have

$$E^2 + f(r_E) = 0\,. \tag{3.4}$$

As in [17], we must have $t_L(r_E) = 0$ and $t_E(r_E) = -\beta/4$. Such geodesics satisfy

$$t_0 + i\frac{\beta}{4} = E\int_{r_E}^{\infty} \frac{\mathrm{d}r}{V(r)\sqrt{E^2 - V(r)}}\,, \tag{3.5}$$

where $V(r)$ is the effective potential described above, for either rotating or non-rotating geodesics. Since the qualitative features are similar, we will only be concerned with the latter, for which $V(r) = -f(r)$.

The two features prominent in the analogous discussion of [17], for the AdS-Schwarzschild metric, are the branch cut at $t_0 = 0$ (corresponding to $E = 0$) and the existence of a critical value $t_0 = -t_c$ (corresponding to $E = \infty$), where the correlators naively diverge. The latter feature was interpreted as a signal of the singularity encoded in gauge theory correlation functions, the former making that encoding a subtle one. In our discussion these features are no longer present. The special values of the energy are $E = 0$ and $E^2 = V_{\max}$, and we discuss them both below.

For general energies, one can compute (3.5) in terms of elliptic integrals,[9] which we do in the appendix. The result will depend both on the roots of the cubic $\Delta(x)$ and on the roots of the other cubic appearing in the denominator of (3.5),

$$\tilde{\Delta}(x) = E^2x^2 + (x + x_0)(x - x_-)(x - x_+) \equiv (x + \tilde{x}_0)(x - \tilde{x}_-)(x - \tilde{x}_+)\,, \tag{3.6}$$

where the roots $\tilde{x}_+ > \tilde{x}_- > 0 > -\tilde{x}_0$ and $\tilde{x}_+ = r_E^2$.

From the appendix, we have[10]

$$\begin{aligned} t_0 = -E\frac{1}{\sqrt{\tilde{x}_+(\tilde{x}_- + \tilde{x}_0)}}\Bigg[&\frac{x_0^3(\tilde{x}_+ - \tilde{x}_-)}{(\tilde{x}_+ + x_0)(\tilde{x}_- + x_0)(x_0 + x_-)(x_0 + x_+)}\ \Pi(\tilde{\phi}, \tilde{\alpha}_0^2, \tilde{k}) + \\ &+ \frac{x_-^3(\tilde{x}_+ - \tilde{x}_-)}{(\tilde{x}_+ - x_-)(\tilde{x}_- - x_-)(x_0 + x_-)(x_+ - x_-)}\ \Pi(\tilde{\phi}, \tilde{\alpha}_-^2, \tilde{k}) - \\ &- \frac{x_+^3(\tilde{x}_+ - \tilde{x}_-)}{(\tilde{x}_+ - x_+)(\tilde{x}_- - x_+)(x_0 + x_+)(x_+ - x_-)}\ \Pi(\tilde{\phi}, \tilde{\alpha}_+^2, \tilde{k}) + \\ &+ \frac{\tilde{x}_-^3}{(\tilde{x}_- + x_0)(\tilde{x}_- - x_-)(\tilde{x}_- - x_+)}\ \mathrm{F}(\tilde{\phi}, \tilde{k})\Bigg]\,, \end{aligned} \tag{3.7}$$

[9] We use the notation of [28] for the elliptic integrals.

[10] This expression is actually valid for *any* geodesic, not just symmetric ones. We simply have to replace t_0 with $t_{\mathrm{b}} - t_{\mathrm{tp}}$, these values denoting, respectively, the values of t_L at the boundary and at the turning point.

JHEP04(2005)004

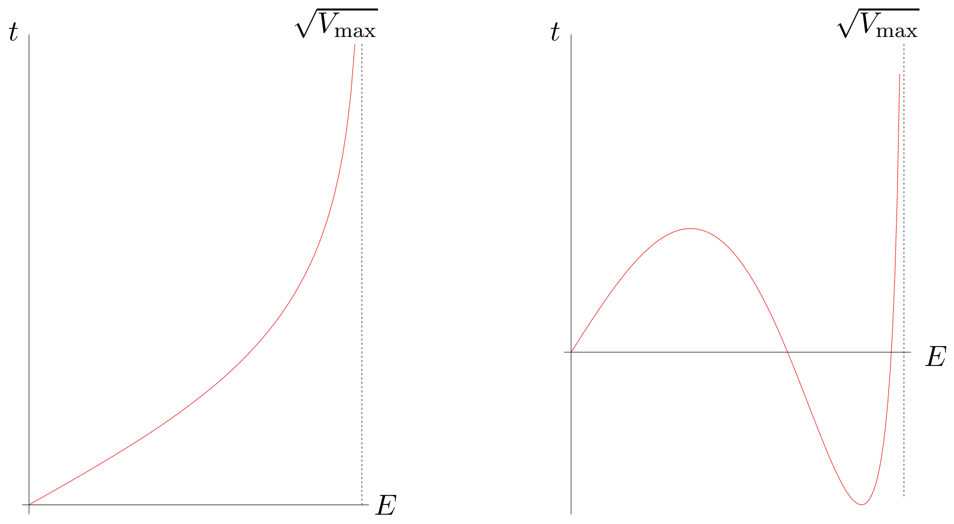

Figure 5: The left-hand plot shows $t(E)$ for $x_+ \sim x_-$ whereas the right-hand plot has $x_+ \gg x_-$. The dotted lines indicate $E^2 = V_{\max}$.

where

$$\tilde{\alpha}_0^2 = \left(\frac{\tilde{x}_+ + \tilde{x}_0}{\tilde{x}_- + \tilde{x}_0}\right)\left(\frac{\tilde{x}_- + x_0}{\tilde{x}_+ + x_0}\right), \qquad \tilde{\alpha}_-^2 = \left(\frac{\tilde{x}_+ + \tilde{x}_0}{\tilde{x}_- + \tilde{x}_0}\right)\left(\frac{\tilde{x}_- - x_-}{\tilde{x}_+ - x_-}\right), \tag{3.8}$$

$$\tilde{\alpha}_+^2 = \left(\frac{\tilde{x}_+ + \tilde{x}_0}{\tilde{x}_- + \tilde{x}_0}\right)\left(\frac{\tilde{x}_- - x_+}{\tilde{x}_+ - x_+}\right), \qquad \tilde{k} = \sqrt{\frac{\tilde{x}_-}{\tilde{x}_+}\left(\frac{\tilde{x}_+ + \tilde{x}_0}{\tilde{x}_- + \tilde{x}_0}\right)}, \qquad \tilde{\phi} = \sin^{-1}\sqrt{\frac{\tilde{x}_- + \tilde{x}_0}{\tilde{x}_+ + \tilde{x}_0}}.$$

Note that this result includes the imaginary part $-i\beta/4$ from crossing the horizon; it arises from a pole in the region of integration in the third term above.

This is a fairly unilluminating expression, but more information can be seen if we plot $t(E)$ numerically, for various choices of black hole parameters. We find two distinct types of behaviour, shown in figure 5:

- The left-hand plot is representative of the behaviour for $x_+ \sim x_-$, where the black hole is near-extreme. The boundary time t is then a monotonically increasing function of energy E.

- The right-hand plot, on the other hand, represents the behaviour for $x_+ \gg x_-$, this limit being one of large mass and small charge.

- In both cases, we clearly see a divergence in t as $E^2 \to V_{\max}$.

There is thus a range of parameter space in which, for each value of boundary time t, there exists a unique geodesic connecting the two boundary points (the left-hand plot in figure 5). However, outside of this range (the right-hand plot in figure 5), there are values of boundary time for which there are multiple geodesics connecting the two boundaries,

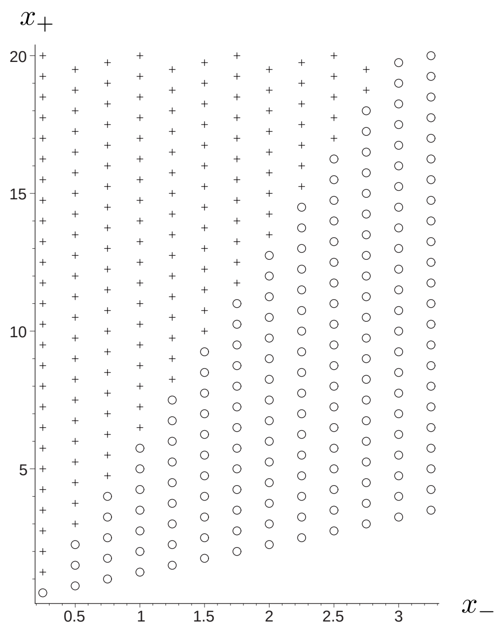

Figure 6: This plot shows how $t(E)$ behaves as a function of the parameters $x_\pm$. Circles denote points for which t is a monotonically increasing function of E, and crosses denote points for which t has a turning point for some value of E.

each with a different value of E. Which one dominates the path integral will depend on the relative proper lengths, though one should be more careful than this: some of these saddle points may not contribute to the path integral at all.

The precise point of cross-over between these two types of behaviour, as a function of parameters, is difficult to pin down analytically but is possible to analyse numerically. For example, figure 6 shows a region of $x_\pm$ parameter space, the circles denoting that t is a monotonically increasing function of E for those choices of parameters, and the crosses denoting that t has a turning point.[11]

It should be clear from this figure that the near-extreme black holes have unique geodesics connecting boundary points, the boundary time t in this case being a single-valued function of the energy E.

Small E geodesics. It is easy to see that $E = 0$ corresponds to $t_0 = 0$, both for rotating and non-rotating geodesics. For $E = 0$, we have

$$\dot{t} = 0 \qquad \Rightarrow \qquad t(\lambda) = 0, \qquad \dot{r}^2 = f(r)\,, \tag{3.9}$$

so these geodesics start at the boundary, pass straight through the Penrose diagram and end at the other boundary, without ever penetrating the horizon.

To derive the small E behaviour of (3.7), we need the E-dependence of the roots $\tilde{x}_0, \tilde{x}_-$ and $\tilde{x}_+$. This is determined by the following set of equations:

$$\tilde{x}_0 - \tilde{x}_- - \tilde{x}_+ = x_0 - x_- - x_+ + E^2\,,$$

[11] It is curious that the boundary between these two types of behaviour is a straight line.

$$\tilde{x}_-\tilde{x}_+ - \tilde{x}_0\tilde{x}_+ - \tilde{x}_0\tilde{x}_- = x_-x_+ - x_0x_+ - x_0x_- \,,$$
$$\tilde{x}_0\tilde{x}_-\tilde{x}_+ = x_0x_-x_+ \,. \tag{3.10}$$

Since we are interested only in small E, we can solve these by taking

$$\begin{aligned} \tilde{x}_0 &= x_0 + (1 + a_- + a_+)E^2 + \mathcal{O}(E^4), \\ \tilde{x}_- &= x_- + a_-E^2 + \mathcal{O}(E^4)\,, \\ \tilde{x}_+ &= x_+ + a_+E^2 + \mathcal{O}(E^4)\,, \end{aligned} \tag{3.11}$$

where

$$a_\pm = \mp\frac{r_\pm}{\kappa_\pm}\,. \tag{3.12}$$

It is important that the possible order E terms in (3.11) necessarily vanish, as long as $x_+ \neq x_-$, which in turn implies that all odd powers of E also vanish. We then have

$$\tilde{\phi} = \phi + \phi_1E^2 + \mathcal{O}(E^4)\,, \qquad \tilde{k} = k + k_1E^2 + \mathcal{O}(E^4)\,, \qquad \tilde{\alpha}^2 = \alpha^2 + \alpha_1^2E^2 + \mathcal{O}(E^4) \tag{3.13}$$

(for each of the $\tilde{\alpha}$s), and where the quantities without a tilde are independent of E, being functions of the roots x_0, x_- and x_+ only. The elliptic integrals can then be Taylor expanded in each of their arguments using the well-known expressions for the various derivatives [28].

The net result is that

$$t_0 = t_1E + \mathcal{O}(E^3) \tag{3.14}$$

for some non-vanishing constant t_1. This expression for $t(E)$ is similar to the finite mass black hole of [17], and in particular is an analytic function near $E = 0$. Moreover, numerical experimentation shows (as in figure 5) that for generic choices of the black hole parameters, the constant $t_1 > 0$. We can generate cases for which $t_1 < 0$, for example by taking $x_- = 0.2$ and $x_+ = 1$, but we have to work quite hard to do this: it seems that we need x_- small. This is just the Schwarzschild limit $x_- \to 0$ and, in that case, we can find both small and large mass (small and large x_+) black holes with $t_1 < 0$. So, although there are black holes with $t_1 < 0$, they are all in the neighbourhood of the neutral hole; we will concentrate on the generic case with $t_1 > 0$.

The regime $E^2 \to V_{\rm max}$. The integrand in (3.5) is divergent at the turning point of the trajectory, where $E^2 = V(r)$. This singularity is integrable for $E^2 \neq V_{\rm max}$, leading to finite boundary time t_0 for $0 < E^2 < V_{\rm max}$. On the other hand, when $E^2 = V_{\rm max}$, the two positive roots of $\tilde{\Delta}(x)$ coincide ($\tilde{x}_+ = \tilde{x}_-$), leading to a logarithmic divergence in (3.5). We emphasise that this is true for both the rotating and non-rotating geodesics.

The divergence is shown clearly in figure 5, but we can see it analytically from the exact result (3.7) in the following way. Take $\tilde{x}_- = \tilde{x}_+ - \varepsilon$ and note that $\tilde{k}$ and each $\tilde{\alpha}^2$ go to one faster than $\tilde{\phi}$ goes to $\pi/2$, since

$$\tilde{k} = 1 + \mathcal{O}(\varepsilon), \qquad \tilde{\alpha}^2 = 1 + \mathcal{O}(\varepsilon)\,, \qquad \tilde{\phi} = \frac{\pi}{2} + \mathcal{O}(\varepsilon^{1/2})\,. \tag{3.15}$$

Then note that

$$\tilde{x}_+ - \tilde{x}_- = \frac{\tilde{x}_+(\tilde{x}_- + \tilde{x}_0)}{\tilde{x}_0}(1 - \tilde{k}^2) \tag{3.16}$$

and use [28]

$$\Pi(\phi, 1, k) = \frac{1}{(1-k^2)}\left((1-k^2)\, F(\phi,k) - E(\phi,k) + \tan\phi\sqrt{1-k^2\sin^2\phi}\right). \tag{3.17}$$

The problematic $(1-k^2)$ factors cancel, giving

$$\begin{aligned} t_0 &= -E\frac{\tilde{x}^{5/2}}{(\tilde{x}_+ + \tilde{x}_0)^{3/2}(\tilde{x}_+ - x_-)(\tilde{x}_+ - x_+)}\ \ln(\tan\tilde{\phi} + \sec\tilde{\phi}) \\ &\sim -\ln(\cos\pi/2) + \text{finite}\,, \end{aligned} \tag{3.18}$$

since $x_- < \tilde{x}_+ < x_+$.

Since the boundary time diverges as $E^2 \to V_{\max}$, the gauge theory does not seem to encode the regime $E^2 > V_{\max}$.

3.3 Correlation functions

The proper length of both the rotating and non-rotating geodesics is given by

$$L = 2\int_{r_E}^{r_{\max}} \frac{\mathrm{d}r}{\sqrt{E^2 - V(r)}} \tag{3.19}$$

with $V(r)$ being the relevant potential in each case. r_E is the same turning point as in the previous subsection and, since we will only be concerned with the non-rotating case, it is again given by solving (3.4). The upper limit, $r_{\max}$, is a long-distance radial cutoff, dual to the UV cutoff in the gauge theory. As we take $r_{\max} \to \infty$, the integral diverges logarithmically. To regularise it we subtract the divergent piece arising in the pure AdS case (obtained by setting $x_0 = 1$ and $x_- = x_+ = 0$ in the above expression). This standard process is dual to renormalisation of the boundary theory [29].

$E = 0$ **geodesics.** We start with the $E = 0$ symmetric geodesics, which approximate the boundary correlators with $t_0 = 0$. The proper length of such a geodesic is

$$L = 2\int_{r_+}^{r_{\max}} \frac{\mathrm{d}r}{\sqrt{f(r)}} = \int_{r_+^2}^{r_{\max}^2} \mathrm{d}x\sqrt{\frac{x}{(x+x_0)(x-x_-)(x-x_+)}}\,, \tag{3.20}$$

where the turning point for $E = 0$ is $r = r_+$, the location of the outer horizon. We can compute (3.20) in terms of elliptic integrals, giving [28]

$$L = \frac{2}{\sqrt{x_+(x_- + x_0)}}\left[x_-\ \mathrm{F}(\phi,k) + (x_+ - x_-)\ \Pi(\phi, x_+k^2/x_-, k)\right], \tag{3.21}$$

where

$$\phi = \sin^{-1}\sqrt{\frac{(x_- + x_0)(r_{\max}^2 - x_+)}{(x_+ + x_0)(r_{\max}^2 - x_-)}}\,, \qquad k = \sqrt{\frac{x_-(x_+ + x_0)}{x_+(x_- + x_0)}} = \sqrt{\frac{\kappa_+}{\kappa_-}\frac{r_+}{r_-}}\,. \tag{3.22}$$

In the limit $r_{\max} \to \infty$, the logarithmic divergence appears in $\Pi(\phi, x_+k^2/x_-, k)$ (whereas $\mathrm{F}(\phi, k)$ remains finite). To extract this divergence, we note that $\alpha^2 = x_+k^2/x_- > 1$, so we can use [30]

$$\Pi(\phi, \alpha^2, k) = -\Pi(\phi, k^2/\alpha^2, k) + \mathrm{F}(\phi, k) + \frac{1}{2p_1} \ln \left(\frac{\Delta(\phi) + p_1 \tan\phi}{\Delta(\phi) - p_1 \tan\phi} \right), \tag{3.23}$$

where $p_1 = \sqrt{(\alpha^2 - 1)(1 - k^2/\alpha^2)}$ and $\Delta(\phi) = \sqrt{1 - k^2 \sin^2\phi}$. Expanding to first order in $1/r^2_{\max}$ gives

$$L = \frac{2}{\sqrt{x_+(x_- + x_0)}} \left[x_+\mathrm{F}(\phi, k) - (x_+ - x_-)\Pi\left(\phi, \frac{x_-}{x_+}, k\right)\right] + \ln\left(\frac{4}{x_0 + x_- + x_+}\right) + \ln(r^2_{\max}) \,, \tag{3.24}$$

the logarithmic divergence being manifest. The renormalised result is thus

$$L_{\mathrm{ren}} = \frac{2}{\sqrt{x_+(x_- + x_0)}} \left[x_+ \; \mathrm{F}(\phi, k) - (x_+ - x_-) \; \Pi(\phi, x_-/x_+, k)\right] + \ln\left(\frac{4}{x_0 + x_- + x_+}\right), \tag{3.25}$$

where now

$$\phi = \sin^{-1} \sqrt{\frac{x_- + x_0}{x_+ + x_0}} \,. \tag{3.26}$$

$0 < E < V_{\max}$ geodesics. As in [17], as we increase the energy, the geodesic will penetrate some distance inside the horizon. The proper length of the (non-rotating) geodesic is now:

$$\mathcal{L} = 2\int_{r_E}^{r_{\max}} \frac{\mathrm{d}r}{\sqrt{E^2 + f(r)}} = \int_{r_E^2}^{r^2_{\max}} \mathrm{d}x \sqrt{\frac{x}{E^2x^2 + (x + x_0)(x - x_-)(x - x_+)}} \tag{3.27}$$

which will depend on the roots of the cubic $\tilde{\Delta}(x)$, defined in (3.6). Formally, the result is as in (3.25), but with the E-dependent roots:

$$L_{\mathrm{ren}} = \frac{2}{\sqrt{\tilde{x}_+(\tilde{x}_- + \tilde{x}_0)}} \left[\tilde{x}_+ \; \mathrm{F}(\tilde{\phi}, \tilde{k}) - (\tilde{x}_+ - \tilde{x}_-) \; \Pi\left(\tilde{\phi}, \frac{\tilde{x}_-}{\tilde{x}_+}, \tilde{k}\right)\right] + \ln\left(\frac{4}{\tilde{x}_0 + \tilde{x}_- + \tilde{x}_+}\right), \tag{3.28}$$

where

$$\tilde{\phi} = \sin^{-1}\sqrt{\frac{\tilde{x}_- + \tilde{x}_0}{\tilde{x}_+ + \tilde{x}_0}}, \qquad \tilde{k} = \sqrt{\frac{\tilde{x}_-(\tilde{x}_+ + \tilde{x}_0)}{\tilde{x}_+(\tilde{x}_- + \tilde{x}_0)}} \,. \tag{3.29}$$

To take the small E limit of this expression, we proceed as in the previous subsection, using the expressions (3.11). The upshot is that

$$L(E) - L(E = 0) = L_1 E^2 + \mathcal{O}(E^4) \tag{3.30}$$

for some non-vanishing constant L_1. Using the previous expression (3.14) for the small E behaviour of the boundary time, we see that

$$L(E) - L(E = 0) \sim t^2 \,. \tag{3.31}$$

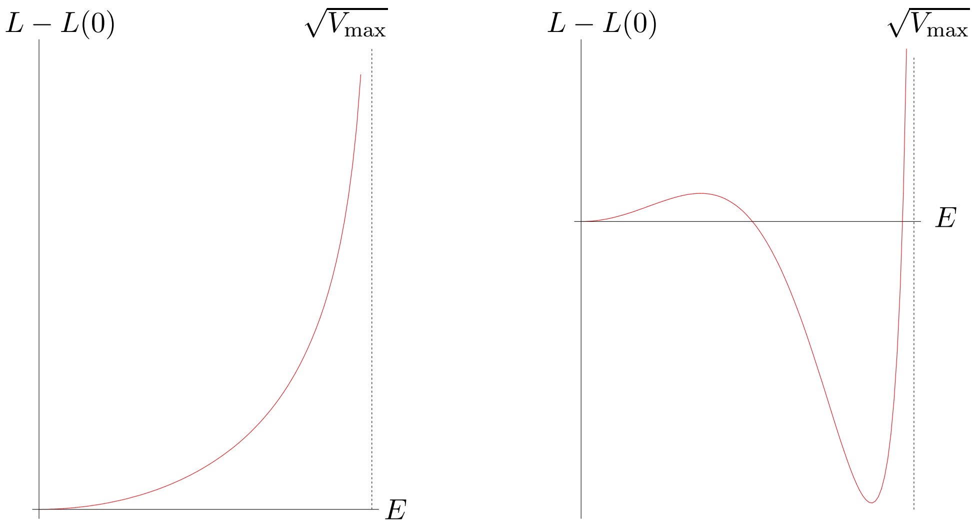

Figure 7: The left-hand plot shows $L(E) - L(E = 0)$ for $x_+ \sim x_-$ whereas the right-hand plot has $x_+ \gg x_-$. The dotted lines indicate $E^2 = V_{\max}$.

The result is therefore analytic around $E = 0$, the branch cut structure found in [17] for the infinitely massive black hole being absent here. It is more similar to the finite mass black hole [17].

On the other hand, as for the computation of the boundary time above, the integral (3.19) will have an additional logarithmic divergence at the lower limit for $E = V_{\max}$, which we can again extract analytically, or observe numerically. In figure 7, we plot $L(E)$, the proper length as a function of energy, for the two different regimes of the previous subsection. The parameters are the same as those in figure 5, the left-hand plot being representative of the behaviour for $x_+ \sim x_-$, and the right-hand plot being representative of the behaviour for $x_+ \gg x_-$. The divergence as $E^2 \to V_{\max}$ can clearly be seen. We emphasize again that the regularized length diverges to $+\infty$, and correspondingly the correlators *decay* exponentially.

There are two important points to note here. Firstly, as shown in figure 7, for generic choices of black hole parameters, we have the constant $L_1 > 0$ in the small E behaviour (3.30). As for the small E behaviour of the boundary time, however, it is possible to arrange that $L_1 < 0$. But, again, these cases seem non-generic and we will concentrate on black holes with $L_1 > 0$. (The black holes in the Schwarschild limit $x_- \to 0$, with $t_1 < 0$ in (3.14), also have $L_1 < 0$ in (3.30).)

In that case, and for near-extreme black holes, it should be clear that the correlator will be bounded by its value at $t_L = 0$. The left-hand plot in figure 7 shows in this case that L is a monotonically increasing function of E, its minimum value indeed being at $E = 0$ (and so at $t_L = 0$). So, at least in this case, there is no contradiction with our field theory intuition. For the black holes far from extremality, however, this is no longer clear, as the right-hand plot in figure 7 shows. As in the neutral case [17], one would have to be more careful to reconcile our plots with the field theory properties.

We will thus concentrate on the generic near-extreme black holes, and have these in mind when we turn to analyse the perturbed spacetimes. Moreover, as we will see in the following subsection, it is indeed the real geodesics that dominate the late time correlators for these near-extreme black holes.

3.4 Euclidean slice

Here we want to show that the real geodesics discussed above dominate the correlation function at $t_L = 0$. We can then plausibly argue, as in [17], that the real geodesics continue to dominate at late times. We will not comment on the subtleties of analytic continuation from the euclidean regime, but we will show — at least for certain choices of black hole parameters — that the real geodesic at $t_L = 0$ has shorter proper length than the complex goedesics, and should thus dominate the correlator.

The euclidean metric is found in the usual way, by setting $t = it_E$. With respect to the geodesics, the effect is simply to take $E = -i\tilde{E}$, where the "Euclidean energy" $\tilde{E}$ is the conserved quantity associated with t_E. It turns out that our expressions (3.7) and (3.28) for the boundary time and proper length are still valid after performing this analytic continuation, both on the explicit E dependence, and on that appearing in the expressions (3.10) for the E-dependent roots. We can then plot the boundary time $t_E(\tilde{E})$ and proper length $L(\tilde{E})$ in the euclidean regime, as we did for the lorentzian case above.

Before presenting these plots, let us analyse the expected small $\tilde{E}$ behaviour. We can derive this from an analytic continuation of the results (3.14) and (3.30) in the lorentzian case, finding

$$t_E(\tilde{E}) = -t_1\tilde{E} + t_2\tilde{E}^3\,, \tag{3.32}$$

$$L(\tilde{E}) - L(0) = -L_1\tilde{E}^2 + L_2\tilde{E}^4\,. \tag{3.33}$$

We argued above that, for generic choices of black hole parameters, we have $t_1 > 0$ and $L_1 > 0$, but the signs of the next-to-leading-order terms are harder to determine. It appears that either sign for both t_2 and L_2 is possible, depending on the black hole parameters.

Either way, at large values of $\tilde{E}$ there is a unique goedesic for each value of t_E. As we decrease $\tilde{E}$, however, and come into the small $\tilde{E}$ domain, other geodesics might appear, as in [17]. From (3.32), it is clear that this will occur when $\tilde{E} \sim \sqrt{t_1/t_2}$. Since we have assumed $t_1 > 0$, we will only encounter a branch point when $t_2 > 0$. Otherwise, there will be a unique geodesic for all $\tilde{E} > 0$.

At precisely $t_E = 0$, there are three solutions of (3.32). We will have geodesics with either $\tilde{E} = 0$, or $\tilde{E} = \pm\sqrt{t_1/t_2}$. The former has zero proper length, and may or may not dominate over the latter two. However, if we consider black holes for which $t_2 < 0$ (and $t_1 > 0$) then we simply never encounter a branch point. There is only ever one branch and we can continue into the lorentzian regime, by taking $t_L > 0$, moving along the single real branch of geodesics. On the other hand, in the case that $t_2 > 0$, the proper length of the

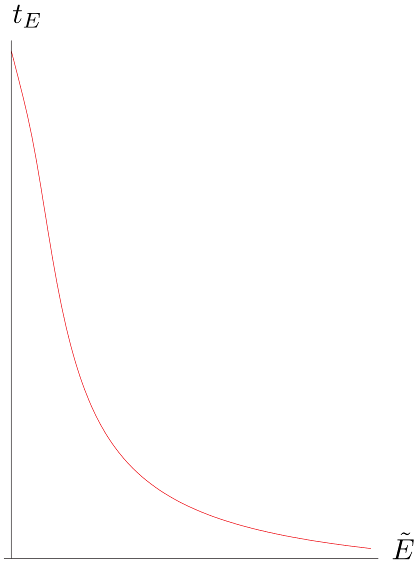

Figure 8: A plot of the boundary time t_E in the euclidean regime, with $x_- = 1, x_+ = 4$. At $\tilde{E} = 0$ we have $t_E = \beta/4$. This type of behaviour — the fact that t_E is single-valued — seems fairly generic.

two geodesics with non-zero $\tilde{E}$ is

$$L = \frac{1}{t_2^2}(L_2 - t_1 L_1 t_2)\,, \tag{3.34}$$

so which geodesics dominate the correlator will depend on the specific values of the various constants.

The important point is that there are black holes with $t_2 < 0$, so that no branch points appear as we take $\tilde{E} \to 0$. We can see that such black holes exist by plotting the Euclidean boundary time $t_E(\tilde{E})$. We find that t_E is generically a single-valued function of $\tilde{E}$, as shown in figure 8, monotonically decreasing from its value $\beta/4$ at $\tilde{E} = 0$. This seems to be true for both near-extreme and far-from-extreme black holes. Other behaviour is possible, however, in that we can find parameters for which t_E is multi-valued. As for our discussion of the small E behaviour in the previous two subsections, it seems that we have to take x_- small to arrange this. And, since taking $x_- \to 0$ is the Schwarzschild limit, we should not be surprised to find such behaviour, since this is what was found in [17]. Away from this limit, however, the picture should be clear.

In fact, we have the stronger result that t_E is generically single-valued for *all* values of $\tilde{E}$, not just in the $\tilde{E} \to 0$ limit. In that case, there is no evident issue with complex branches, and the real geodesic will dominate the late time correlators. We note also that these conclusions hold for sufficiently large black holes, even in the near-neutral case.

3.5 Behaviour at finite t_L

We have found that the subtle features of the infinitely massive AdS-Schwarzschild black hole are likely to be absent in our calculation. This is not surprising, since even very far from extremality we are expected to reproduce only the features of the finite mass black hole. The simplest scenario is that the real geodesics dominate the behavior of the correlation function both at early and late times.

On the other hand, one may worry that some change of behaviour (such as crossing of anti-Stokes lines) can occur at finite t_L, causing the real geodesic we are interested in to be subdominant at late times. This is a subtle question which we do not have a general answer for. However, we observe that for some black hole parameters, and for some region of boundary times, there are multiple *real* geodesics connecting the same boundary points. As we are interested mainly in the late time geodesics and their perturbations, we will concentrate on such black holes which do not exhibit this behaviour. As we have seen, those are the black holes which are close enough to being extreme.

For large enough boundary time, there is always a unique geodesic connecting the boundary points. As we decrease the value of the boundary time, there is a critical time $t_{\rm crit}$ (and corresponding energy $E_{\rm crit}$) for which additional geodesics appear. This is seen in the right-hand plot of figure 5, for the case of a black hole far enough from extremality.

4. Charged correlation functions

We now discuss correlation functions of charged operators. As the analytic expressions are significantly more involved, we confine ourselves to discussing the qualitative features of the correlators, which are fairly similar to the neutral case discussed above.

To approximate correlators of operators which carry R-charge, we need to discuss trajectories of electrically charged particles[12]. We will only consider radial motion here, the addition of angular momentum having much the same effect as in the uncharged case[13]. The lagrangian describing such a particle with charge q and unit mass is

$$\mathcal{L} = \frac{1}{2} g_{\mu\nu}\dot{X}^\mu \dot{X}^\nu + qA_\mu \dot{X}^\mu = \frac{1}{2}\left(-f(r)\dot{t}^2 + \frac{\dot{r}^2}{f(r)}\right) - \frac{\mathcal{Q}}{r^2}\dot{t}\,, \tag{4.1}$$

where we have defined $\mathcal{Q} = cqQ$.

The worldline hamiltonian $\mathcal{H} = (-f(r)\dot{t}^2 + f^{-1}(r)\dot{r}^2)/2$ is conserved, since the action is time translation invariant on the worldline. As we are interested in spacelike paths we can rescale λ to set $\mathcal{H} = 1/2$. The equations of motion are then

$$\dot{t} = \frac{1}{f(r)}\left(E - \frac{\mathcal{Q}}{r^2}\right), \qquad \dot{r}^2 = \left(E - \frac{\mathcal{Q}}{r^2}\right)^2 + f(r)\,. \tag{4.2}$$

[12] Such particles exhibit interesting phenomena such as Schwinger pair production and induced emission [31]. See, e.g., [32] and, for a recent discussion, [33]. The Schwinger effect in curved space is studied in [34].

[13] As in that case, for an arbitrarily small angular momentum, one can find trajectories probing the region beyond the Cauchy horizon, but they return to a copy of the boundary on the same side of the Penrose diagram. These are therefore irrelevant to the two-sided correlators discussed here, and more generally we expect such trajectories not to dominate any gauge theory correlator.

Note that shifting A_t by a constant (denoted in section 1 by Φ), which is just a gauge transformation, uniformly shifts the energy of all trajectories. This gauge freedom was fixed above, so that A_t vanishes at the outer horizon. We choose here to absorb the constant part of A_t, into the definition of E.

The relations following from (4.2) are as follows. First, the (real part of) the boundary time, for symmetric trajectories, is

$$t_0 = \int_{r_E}^{\infty} \mathrm{d}r \frac{(E - \frac{\mathcal{Q}}{r^2})}{V(r)\sqrt{(E - \frac{\mathcal{Q}}{r^2})^2 - V(r)}}\,, \tag{4.3}$$

where r_E is the turning point described below. The length of the corresponding trajectory is given by

$$L = 2\int_{r_E}^{r_{\max}} \frac{\mathrm{d}r}{\sqrt{(E - \frac{\mathcal{Q}}{r^2})^2 - V(r)}}\,, \tag{4.4}$$

where $r_{\max}$ is the long distance bulk cutoff introduced in section 3.

The equation for $r(\lambda)$ given in (4.2) cannot be interpreted as describing a particle with energy E^2 moving in a potential $V(r)$, since now the potential itself depends on E. However, one can still describe the qualitative features of the trajectory, which now depend on both the parameters $\mathcal{Q}$ and E.

The turning point, r_E, of the trajectory is the largest root of the equation

$$\left(E - \frac{\mathcal{Q}}{r^2}\right)^2 - V(r) = 0. \tag{4.5}$$

To visualise the situation, in figure 9 we plot $V(r) = -f(r)$ and the (positive semi–definite) function $(E - \mathcal{Q}/r^2)^2$, the behaviour of which depends on the sign of $\mathcal{Q}/E$. We therefore plot the function for both signs.

In either case, there are three possibilities:

- The graphs do not intersect, and there is no classical turning point. These classical trajectories end at the singularity.

- The graphs intersect twice, in which case the turning point is that intersection with the largest value of r. As in the uncharged case, this will always be in the region between the inner and outer horizons.

- The borderline case, in which there is a single intersection point, now not necessarily at precisely the top of the potential. Similar to the discussion above, looking at the behaviour of (4.3) and (4.4) near r_E reveals logarithmic divergences both in the boundary time and in the proper proper length of the geodesics. Therefore this value of E should be viewed as a limiting value, trajectories with larger value of E being irrelevant for our purposes.

These features of $r(\lambda)$ are similar to those discussed previously. It is clear that only those trajectories with a radial turning point will return to a boundary, but it is not clear which boundary this will be. To determine which trajectories are relevant for our two-sided

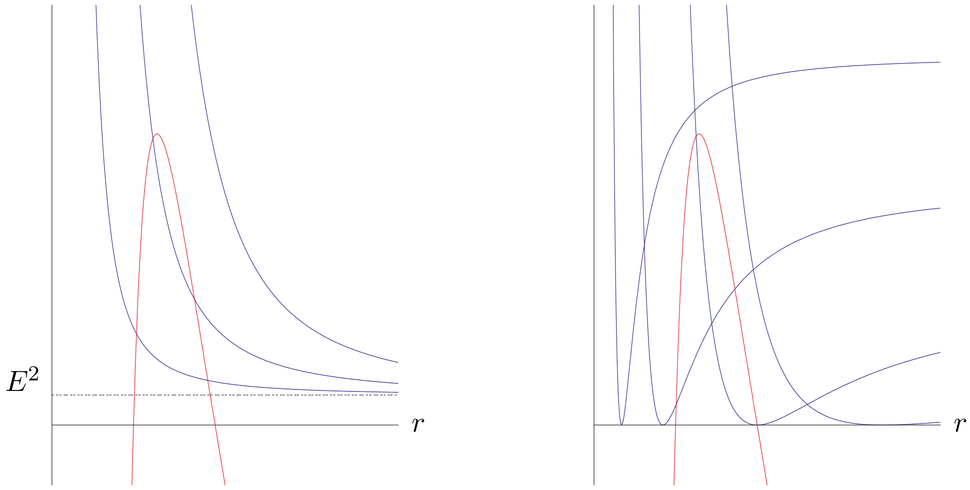

Figure 9: The left-hand plot has $\mathcal{Q}/E < 0$. $V(r) = -f(r)$ is in red and $(E - \mathcal{Q}/r^2)^2$ in blue. Three trajectories with the same energy, E^2, but different charges, are shown. The right-hand plot has $\mathcal{Q}/E > 0$, and shows four trajectories with various values of the parameters. One has $\mathcal{Q}/E > r_+^2$ without a radial turning point, one has $\mathcal{Q}/E = r_+^2$ and two have $\mathcal{Q}/E < r_-^2$, one with a radial turning point and one without.

correlators, we must also consider the behaviour of $t(\lambda)$, which is more involved than in the uncharged case. Let us take $E > 0$ so that t increases with affine parameter from the initial boundary.[14] Then, for $\mathcal{Q} < 0$ (the particle having a charge of opposite sign to the black hole), $\dot{t}$ just depends on the sign of the function $f(r)$: for $r > r_+$ it is positive, whereas for $r_- < r < r_+$ it is negative. So, if such trajectories have a radial turning point, and they do for small enough $\mathcal{Q}$, then they *will* connect the two boundaries of interest. In this case the coordinate $t(\lambda)$ is similar to the neutral geodesics.

The situation for $\mathcal{Q} > 0$ (the particle having a charge of the same sign as the black hole), is more complicated. The behaviour depends on the magnitude of $\mathcal{Q}/E$, and in each case is given by inspection of the right-hand side of the equation for $t(\lambda)$ in (4.2):

- For $\mathcal{Q}/E > r_+^2$, there is some $r > r_+$ for which $\dot{t} = 0$, and the trajectory will start to move backward in coordinate time before reaching the outer horizon. It crosses the event horizon, upon which it moves forward in coordinate time again. If such trajectories have a radial turning point (and some certainly do), then they will connect the two boundaries of interest.

- For $\mathcal{Q}/E = r_+^2$, $\dot{t} = 0$ precisely at the outer horizon, where the particle will necessarily have a radial turning point. It will then return to the same boundary, so such trajectories are of no concern to us.

[14] Trajectories with $E < 0$, but the same sign of $\mathcal{Q}/E$, will just be mirror images of the trajectories we consider.

- For $r_-^2 \leq \mathcal{Q}/E < r_+^2$, $\dot{t}$ does not vanish unless $r_- < r < r_+$. However, it necessarily has a radial turning point *before* the radius at which $\dot{t} = 0$, so will indeed connect the two boundaries of interest.
- Finally, for $\mathcal{Q}/E < r_-^2$, the particle may or may not have a radial turning point. If it does, then it will connect the boundaries of interest. Otherwise, the sign of $\dot{t}$ will flip at some $r < r_-$, and the trajectory will always hit the singularity.

The qualitative behaviour of the charged trajectories which do connect the two boundaries is thus similar to the neutral spacelike geodesics analysed above. They never cross the Cauchy horizon and, again, only reach a radius strictly larger than r_-.

5. Scanning behind the horizon

5.1 Perturbing the AdS-RN spacetime

When the charged black hole is perturbed, linearised analysis suggests strong back-reaction near the inner horizon [1]–[3]. This is one instance of physics behind the horizon which would be nice to interpret in the gauge theory. We take here some preliminary steps towards this goal, postponing a more complete discussion for [26].

First, if one restricts attention to null perturbations which are either purely ingoing, or purely outgoing[15] (i.e., they are chiral in the sense of [35]), then one can solve for the perturbed metric exactly [25, 26]. One obtains an AdS version of the charged Vaidya solution [36, 25]. This solution contains one arbitrary function (the mass function) which depends on the profile of the perturbation. That profile can be varied, and can be arbitrarily localised.[16] By investigating the two-sided correlators (and other observables) as a function of the perturbation, one obtains an efficient method of scanning (at least some of) the region behind the horizon. We will demonstrate here the effects on our observables of a simple wave profile, that of an infinitely localised delta function pulse.

Secondly, in the asymptotically flat case, when both types of null perturbations are turned on[17] the spacetime is drastically changed near the inner horizon, resulting in the phenomenon of *mass inflation* [25]. We expect that this phenomenon persists in the asymptotically AdS case [37, 26]. We further expect that the dependence of some gauge theory observables will be non-analytic as a function of the perturbation strength: taking that strength to be arbitrarily weak does not diminish its effect.

Such non-analytic behaviour is not uncommon in field theories, and results from the existence of infra-red divergences. When re-summing perturbation theory, one discovers non-analytic dependence on coupling constants. Such behaviour would be slightly surprising for gauge theory on a compact space (a three-sphere in this case), at finite temperature and density, but it may be sensible in the infinite N limit.

[15]For a massless field in AdS space, there are two types of perturbations, the non-normalisable one goes to a constant near the boundary. These are the type of perturbations we consider here. In the gauge theory this corresponds to turning on a marginal perturbation, with a specific time-dependent profile.

[16]This arbitrariness is similar to gravitational plane waves which solve Einstein's equation for an arbitrary wave profile.

[17]These are still not generic perturbations, so cosmic censorship considerations do not apply.

Here, we find a behaviour which is perhaps more sensible. As we saw above the spacelike geodesics accumulate at some finite distance from the Cauchy horizon. This is no longer necessarily true of the perturbed geometry. Nevertheless the geodesics we investigate seem to always be screened from the dramatic behaviour at the Cauchy horizon, as is demonstrated below. It is unclear if this is a property of the particular observables we are studying, or a more general property of the gauge theory.

An asymptotically AdS charged Vaidya solution. The Vaidya solution [36] describes an ingoing or outgoing null shell of matter incident on a vacuum black hole. Poisson and Israel generalised this to include charge in [25], their aim being to investigate the properties of the Cauchy horizon of the asymptotically flat Reissner-Nordström black hole. It is easy to further generalise these solutions to the asymptotically AdS case. In fact, though we will not do this here, one can derive [26] asymptotically AdS versions of the solutions relevant to mass inflation [25], describing both ingoing and outgoing flux.

In terms of the lightcone coordinate $u = t - r_*$ defined in section 2, the outgoing solution, in the region $r_- < r < r_+$, has the metric

$$\mathrm{d}s^2 = -f(u,r)\mathrm{d}u^2 - 2\mathrm{d}u\mathrm{d}r + r^2\mathrm{d}\Omega_3^2\,, \tag{5.1}$$

where all the u-dependence in the metric function is through that of the mass function $M(u)$:

$$f(u,r) = 1 - \frac{M(u)}{r^2} + \frac{Q^2}{r^4} + r^2\,. \tag{5.2}$$

The u-dependence is set by the flux sent in from the left-hand boundary, which must have the null energy-momentum tensor, whose only non-zero component is

$$T_{uu} = \frac{1}{2}\frac{\partial_u M(u)}{r^3}\,. \tag{5.3}$$

It is easy to check that this metric and energy-momentum tensor, together with the background gauge field given in (2.1) solve the five dimensional Einstein-Maxwell field equations with negative cosmological constant.

A simple example. The simplest case, which we will consider here, is to take

$$M(u) = m_1 + \Theta(u - u_p)\Delta m\,. \tag{5.4}$$

The corresponding energy-momentum tensor

$$T_{uu} = \frac{\Delta m}{2}\frac{\delta(u - u_p)}{r^3} \tag{5.5}$$

corresponds to an infinitely thin shell of null matter, the flux leaving the left-hand boundary at $t = t_p$. The spacetime splits into two regions: for $u < u_p$ the mass is m_1 and for $u > u_p$, the mass is $m_2 = m_1 + \Delta m$. We can then apply the previous analysis to the two regions, each with its own potential, and match across the $u = u_p$ surface. For non-rotating neutral geodesics the potential in each region is simply $V(r) = -f_{m_{1,2}}(r)$, where $f_m(r)$ is the radial function (5.2) with specific value of the mass parameter m.

JHEP04(2005)004

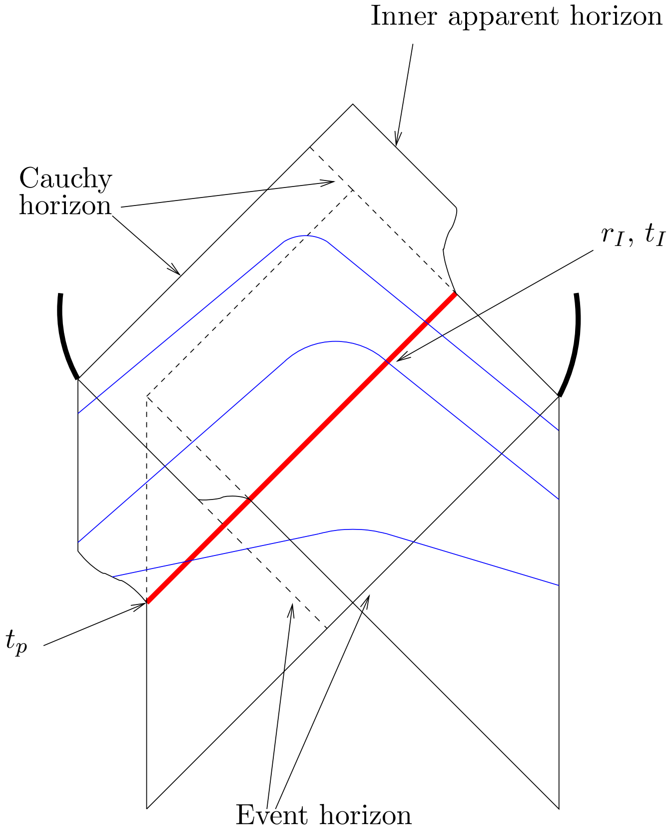

Figure 10: The geometry of the perturbed spacetime, showing the event horizon, the Cauchy horizon and the inner apparent horizon. The perturbation leaves the left-hand boundary at $t = t_p$, and is shown as a solid red line. Spacelike geodesics are shown schematically in blue, the point at which they interact with the perturbation being shown as r_I, t_I.

If we take $\Delta m > 0$, then $f_{m_2} < f_{m_1}$ for all values of r. The roots $x_-(m_2)$ and $x_+(m_2)$ of f_{m_2} will thus be respectively less than $x_-(m_1)$ and greater than $x_+(m_1)$. The resulting geometry is shown schematically in figure 10.

Now, to see the effect of the perturbation on the gauge theory, consider again the two-sided correlator in the geodesic approximation. The perturbation is then encoded in properties of spacelike geodesics which intersect the surface $u = u_p$. Some possible geodesics are shown schematically in figure 10, in which we denote the intersection point by r_I, t_I. The interaction with the flux will change the path of the geodesic beyond this intersection point. We are only interested in those geodesics which intersect the flux in the region beyond the outer horizon and it is clear that late-time correlators will be most suitable.

As we change the time t_p at which the pulse leaves the boundary, the intersection point will change, and so will the length L of any geodesic. We should thus be able to see how the correlator changes as a function of t_p, a clear signal of physics behind the horizon. We demonstrate here how the information about the perturbation can be detected in our simple example.

The only subtlety[18] is that the energy of the geodesics is no longer conserved as they cross the null shell. In the first region, from the metric (5.1), the conserved quantity is

$$E = -\frac{1}{2}\frac{\partial \mathcal{L}}{\partial \dot{u}} = f(r)\dot{u} + \dot{r} \tag{5.6}$$

which is equal to the conserved energy $E = -\frac{1}{2}\frac{\partial \mathcal{L}}{\partial \dot{t}}$ in the t, r coordinates we have been using for the unperturbed geometry. In the perturbed case, however, E is no longer conserved: if we define $E \equiv f(r,u)\dot{u} + \dot{r}$ then, from the geodesic equations,

$$\frac{\mathrm{d}E}{\mathrm{d}\lambda} = \frac{1}{2}\partial_u f(r,u)\dot{u}^2 \tag{5.7}$$

which, for the mass function as in (5.4), gives

$$\mathrm{d}E = -\frac{1}{2}\frac{\Delta m}{r^2}\delta(u-u_p)\,\dot{u}\,\mathrm{d}u\,. \tag{5.8}$$

Whereas the "energy" E is discontinuous across the null shell, the momentum normal to the shell, which is just $p_\perp = \dot{u}$, *is* continuous at the interaction point [38]. We can thus integrate the above equation, taking $\dot{u} = \dot{u}(m_1)$, the value of the momentum in the region with mass m_1. From the definition of E, and using the lagrangian constraint $\mathcal{L} = 1$ for spacelike geodesics, we have

$$\dot{u} = \frac{E}{f(r,u)}\left(1 \pm \sqrt{1 + \frac{f(r,u)}{E^2}}\right), \tag{5.9}$$

so that

$$E_2 - E_1 = -\frac{1}{2}\frac{\Delta m}{r_I^2}\frac{E_1}{f_{m_1}(r_I)}\left(1 \pm \sqrt{1 + \frac{f_{m_1}(r_I)}{E_1^2}}\right), \tag{5.10}$$

where E_1 and E_2 denote the respective energies in the regions with mass m_1 and m_2. Note that $f(r_I, u_p) < 0$ so that $E_2 > E_1$.

5.2 Detecting the perturbation

Qualitative features. To analyse the qualitative properties of the geodesics, we reconsider the particle mechanics problem of section 3. The particle moves from the right-hand asymptotic region to the intersection point at $r = r_I$ in the effective potential $V_{m_1}(r) = -f_{m_1}(r)$, and with energy E_1. After the intersection point, the particle continues on its motion, but now in the effective potential $V_{m_2}(r) = -f_{m_2}(r)$, and with energy E_2. The various possibilities are shown in figure 11, in which we fix the energy of the geodesic, and vary the mass, which in turn changes the potential. We can vary the intersection point by varying t_p. There are then three possibilities (we will assume that the particle continues its motion entirely in V_{m_2} after the intersection, i.e. that it does not intersect the pulse a second time):

[18] As pointed out to us by Simon Ross.

- If the intersection point satisfies $r_I > r_E(m_2)$, the turning point of the motion in $V_{m_2}(r)$, then the particle continues its motion in the modified potential until reaching the new turning point $r_E(m_2)$, and will thus still return to the opposite boundary. This is shown in the left-hand plot in figure 11.
- The centre plot has $r_I < r_E(m_2)$, so that after the interaction, it seems that the particle would be moving *below* $V_{m_2}(r)$. However, the new energy in the second region is $E_2 > E_1$, and this shift in the energy across the null pulse is sufficient to cause the particle to jump back above the second potential (we have checked that the shift in energy is large enough for a range of black hole parameters). This case is thus qualitatively similar to the previous one.
- The right-hand plot shows two ingoing particles, both with $E_1^2 > V_{\max}(m_1)$, so they would have fallen into the singularity in the unperturbed case. Here, however, they still have $r_I > r_E(m_2)$, so will continue their motion until reaching this turning point. Contrary to the unperturbed case, such geodesics will thus return to the opposite boundary.

The last case is interesting, since the trajectories now seem to cross the Cauchy horizon. However, as shown schematically in figure 10, by studying the trajectories more carefully one can see that this does not really happen. The trajectories cross the left-hand branch of the surface $r_-(m_1)$, which would have been the Cauchy horizon in the unperturbed spacetime, but is not in the perturbed case. The geodesics never cross the surface $r_-(m_2)$, which is the left-hand branch of the Cauchy surface in this case. Once again, it seems that the correlators are geometrically protected from the catastrophic instability of the Cauchy horizon.

To demonstrate the scanning process of the region behind the event horizon, we will study the features of geodesics which fall into the first class discussed above, those with $E_1^2 < V_{\max}(m_1)$ which intersect the flux at $r_I > r_E(m_2)$. Such geodesics connect both boundaries of the perturbed spacetime, and therefore dominate the correlation functions of the perturbed gauge theory.

A quantitative plot of the correlators. It is difficult to solve analytically for the behaviour of the correlator in the perturbed spacetime. Instead we demonstrate the process by numerically plotting the length of the geodesic as a function of t_p, the time of the perturbation.

Specifically , we plot here the fractional change in the length of the geodesic as a function of t_p,

$$\delta L = \frac{L(\Delta m) - L(\Delta m = 0)}{L(\Delta m = 0)}\,. \tag{5.11}$$

The method to generate the plot is not entirely obvious, so we outline it before presenting the result.

We first fix the initial roots, $x_\pm(m_1)$, of the potential $V_{m_1}(r)$, which fixes the initial mass m_1 and the charge (which remains unchanged). We fix Δm, the strength of the perturbation, which fixes the final mass m_2, and also the new roots $x_\pm(m_2)$ of the potential

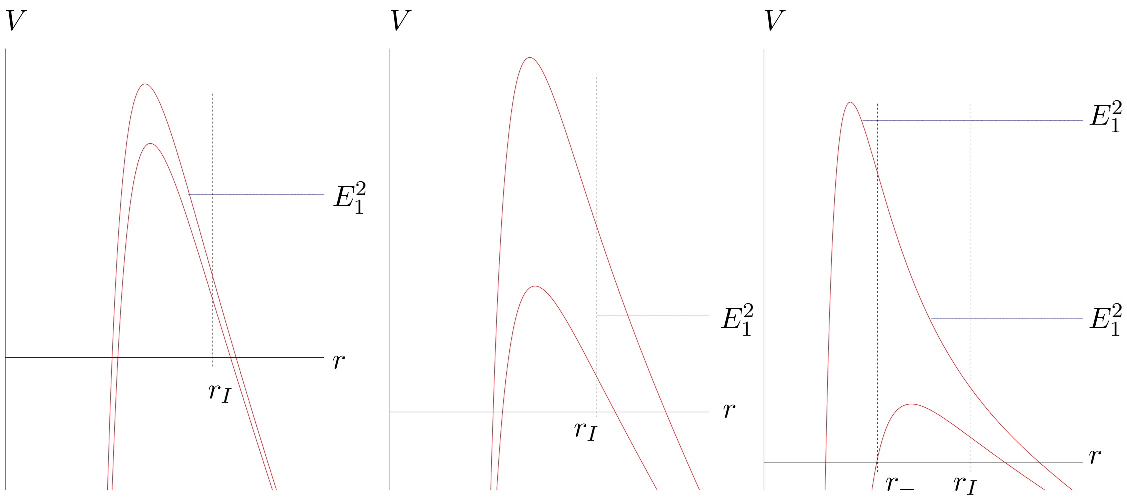

Figure 11: The particles with energy E_1^2 are initially moving in the smaller potential, $V_{m_1}(r)$. They interact with the perturbation at some $r = r_I < r_+(m_1)$, inside the outer horizon, at which point the energy jumps to $E_2^2 > E_1^2$, and they continue to move in the larger potential, $V_{m_2}(r)$. The various possibilities shown are discussed in the text.

$V_{m_2}(r)$. Finally, we fix the initial energy E_1^2 of the geodesic in the unperturbed geometry, which fixes the boundary time of the correlator in that case. We take $E_1^2 \sim V_{\max}(m_1)$ to give late time geodesics, which should be guaranteed to interact with the perturbation in the relevant region.

In the unperturbed spacetime, with mass m_1, the geodesic with energy E_1^2 connects two specific points on opposite boundaries. The proper length of this approximates the correlator of operators inserted at these points. We need to compare this with the correlator in the perturbed spacetime, which *connects the same two points*. The correlators we compute before and after perturbing the spacetime should be the same; in the geodesic approximation, however, they are dominated by geodesics with different energies, say energy $\tilde{E}_1^2$ in the first region of the perturbed geometry (and, as discussed above, with a shifted energy $\tilde{E}_2^2$ in the second region).

Let us denote the points on the left- and right-hand boundaries which the geodesics connect as t_l and t_r. In the unperturbed spacetime, we have

$$t_l(m_1) + t_r(m_1) = 2E_1 \int_{r_{E_1}(m_1)}^{\infty} \frac{\mathrm{d}r}{V_{m_1}(r)\sqrt{E_1^2 - V_{m_1}(r)}}\,, \tag{5.12}$$

which can be computed as in subsection 3.2. This must be equal to the same quantity in the perturbed spacetime:

$$\begin{aligned} t_l(m_2) + t_r(m_1) = {} & \tilde{E}_1 \int_{r_{\tilde{E}_1}(m_1)}^{\infty} \frac{\mathrm{d}r}{V_{m_1}(r)\sqrt{\tilde{E}_1^2 - V_{m_1}(r)}} - \tilde{E}_1 \int_{r_{\tilde{E}_1}(m_1)}^{r_I} \frac{\mathrm{d}r}{V_{m_1}(r)\sqrt{\tilde{E}_1^2 - V_{m_1}(r)}} + \\ & + \tilde{E}_2 \int_{r_{\tilde{E}_2}(m_2)}^{\infty} \frac{\mathrm{d}r}{V_{m_2}(r)\sqrt{\tilde{E}_2^2 - V_{m_2}(r)}} + \end{aligned}$$

$$+\tilde{E}_2\int_{r_{\tilde{E}_2}(m_2)}^{r_I}\frac{\mathrm{d}r}{V_{m_2}(r)\sqrt{\tilde{E}_2^2-V_{m_2}(r)}} \tag{5.13}$$

as can be seen by inspection of figure 10, and where $\tilde{E}_2$ is related to $\tilde{E}_1$ as in (5.10). Again, we can compute this in terms of elliptic integrals as in subsection 3.2. In the perturbed case the result is a function of the intersection radius r_I. Equating the two expressions for the boundary time (5.12), (5.13) in principle gives then a relation $r_I(\tilde{E}_1)$. In practice, however, we need to know the interaction radius to compute $\tilde{E}_2$ (through (5.10)), which in turn we need to compute the interaction radius.

We can avoid this vicious circle by running through values of r_I (knowing that $r_+(m_1) > r_I > r_-(m_2)$) for each $\tilde{E}_1$, computing $\tilde{E}_2$ at each step (we take the smaller solution, with the negative sign in (5.10), to ensure $\tilde{E}_2^2 < V_{\max}(m_1)$), then comparing the two expressions (5.12), (5.13) for these specific values. If they are close enough, then we know that we have the correct value for r_I. Numerical experiment for various values of the black hole parameters shows that the difference between the two expressions (5.12), (5.13) for the boundary time is initially negative, for $r_I \sim r_+(m_1)$, and goes positive for $r_I \sim r_-(m_2)$. So we are guaranteed a value of r_I for which the two expressions are identical, and we simply take that value for which they are closest.

We can use the resulting relation $r_I(\tilde{E}_1)$ to plot the proper length, L, and the time at which the spacetime is perturbed, t_p, as functions of $\tilde{E}_1$. The proper length of the geodesic in the perturbed spacetime is

$$\begin{aligned}L(\Delta m) = &\int_{r_{\tilde{E}_1}(m_1)}^{\infty}\frac{\mathrm{d}r}{\sqrt{\tilde{E}_1^2-V_{m_1}(r)}}-\int_{r_{\tilde{E}_1}(m_1)}^{r_I}\frac{\mathrm{d}r}{\sqrt{\tilde{E}_1^2-V_{m_1}(r)}}+\\ &+\int_{r_{\tilde{E}_2}(m_2)}^{\infty}\frac{\mathrm{d}r}{\sqrt{\tilde{E}_2^2-V_{m_2}(r)}}+\int_{r_{\tilde{E}_2}(m_2)}^{r_I}\frac{\mathrm{d}r}{\sqrt{\tilde{E}_2^2-V_{m_2}(r)}}\end{aligned} \tag{5.14}$$

and the time t_p is

$$\begin{aligned}t_p = &E_1\int_{r_{E_1}(m_1)}^{\infty}\frac{\mathrm{d}r}{V_{m_1}(r)\sqrt{E_1^2-V_{m_1}(r)}}-\tilde{E}_1\int_{r_{\tilde{E}_1}(m_1)}^{\infty}\frac{\mathrm{d}r}{V_{m_1}(r)\sqrt{E_1^2-V_{m_1}(r)}}\\ &+\tilde{E}_1\int_{r_{\tilde{E}_1}(m_1)}^{r_I}\frac{\mathrm{d}r}{V_{m_1}(r)\sqrt{\tilde{E}_1^2-V_{m_1}(r)}}-r_*(r_I)+r_*(\infty).\end{aligned} \tag{5.15}$$

Both expressions can, again, be evaluated in terms of elliptic integrals as in section 3. Both L and t_p are functions of $\tilde{E}_1$, utilising the relation $r_I(\tilde{E}_1)$ found previously.

To recap, we run through values of $\tilde{E}_1$, then run through values of r_I at each step, computing $\tilde{E}_2$, and evaluating (5.12) and (5.13). We find a relation $r_I(\tilde{E}_1)$ by taking those values of r_I for which (5.12) and (5.13) are approximately equal, then evaluate L and t_p for each $\{\tilde{E}_1, r_I\}$. It is then a simple matter to plot the function $\delta L(t_p)$ as given in (5.11). The result is shown in figure 12. This schematic plot is for some specific values of the parameters ($x_- \sim 0.25, x_+ \sim 2.5$, which gives $m_1 = 10$ and $Q = 1.5$, $\Delta m = 0.5$ and $E^2 \sim 0.999 V_{\max}(m_1)$), but it seems to be representative of the general behaviour.

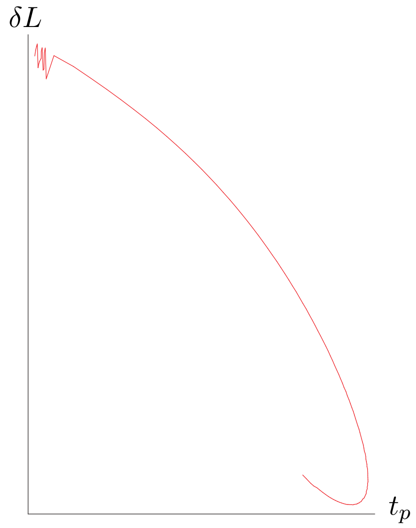

Figure 12: Here we show the fractional change in the length of the geodesic as a function of t_p, for some choice of parameters as explained in the text. The lack of smoothness for small t_p is due to numerical effects, and is not expected to be physical.

This plot demonstrates that our correlators are sensitive to a perturbation of the geometry which is localised beyond the outer horizon. We postpone further discussion for future work, and conclude by making a few comments.

First, we should note that figure 12 cannot be used for the region $V_{\max}(m_1) < \tilde{E}_1^2 < V_{\max}(m_2)$ of energies, since in this case the integrals have to be evaluated differently. Similar methods should work to generate a plot of $\delta L(t_p)$ for that range of energies however.

Moreover, we can only probe part of the region of the spacetime beyond the event horizon. There are no real solutions for r_I beyond a certain range of energies, and this range does not cover the entire region behind the event horizon.

Finally, it is intriguing that the plot of $L(t_p)$ in figure 12 is not single-valued. This means that there are two geodesics, with different energies $\tilde{E}_1$, which connect the fixed boundary points in the perturbed spacetime. Similar to the case of the unperturbed spacetime, this is reflected in some non-analytic behaviour of the correlators in the perturbed spacetime. It would be nice to get a better handle, through analytic calculations, on these issues.

Acknowledgments

We would like to thank Micha Berkooz, Don Marolf, Simon Ross, Paul Saffin and Kristin Schleich for discussions, and are grateful to Simon Ross for pointing out an error in the initial version of this paper. D.B. is supported in part by a postdoctoral fellowship from the Pacific Institute for the Mathematical Sciences. M.R. would like to thank the Physics Departments of Cornell and Syracuse Universities and the KITP in Santa Barbara for hospitality during the course of this work, which was supported in part by the Natural Sciences and Engineering Council of Canada and the National Science Foundation under Grant No. PHY99-07949.

A. The $t(E)$ integral

Consider the integral (3.5) for non-rotating geodesics. Then $V(r) = -f(r)$ and, dropping the residue coming from integrating over the horizon, we have

$$-t_0 = \frac{E}{2}\int_{\tilde{x}_+}^{\infty} \mathrm{d}x \frac{x^{5/2}}{(x+x_0)(x-x_-)(x-x_+)\sqrt{(x+\tilde{x}_0)(x-\tilde{x}_-)(x-\tilde{x}_+)}} \,. \tag{A.1}$$

Defining a new variable t through

$$t^2 = a\left(\frac{x-\tilde{x}_+}{x-\tilde{x}_-}\right), \tag{A.2}$$

with a a constant to be determined, gives

$$-t_0 = \frac{E}{2}A\int_0^a \mathrm{d}t \left(1-\frac{\tilde{c}_0}{a}t^2\right)^{-1/2}\left(1-\frac{\tilde{x}_-}{a\tilde{x}_+}t^2\right)^{5/2}\left(\left(1-\frac{c_0}{a}t^2\right)\left(1-\frac{c_-}{a}t^2\right)\left(1-\frac{c_+}{a}t^2\right)\right)^{-1}, \tag{A.3}$$

where we have set

$$\begin{aligned} A &= \frac{2\tilde{x}_+^{5/2}}{a^{1/2}(\tilde{x}_+ + \tilde{x}_0)^{1/2}}\left((\tilde{x}_+ + x_0)(\tilde{x}_+ - x_-)(\tilde{x}_+ - x_+)\right)^{-1}, \\ \tilde{c}_0 &= \frac{\tilde{x}_- + \tilde{x}_0}{\tilde{x}_+ + \tilde{x}_0}, \qquad c_0 = \frac{\tilde{x}_- + x_0}{\tilde{x}_+ + x_0}, \qquad c_- = \frac{\tilde{x}_- - x_-}{\tilde{x}_+ - x_-}, \qquad c_+ = \frac{\tilde{x}_- - x_+}{\tilde{x}_+ - x_+}. \end{aligned} \tag{A.4}$$

Now observe that

$$\begin{aligned} &\left(\left(1-\frac{c_0}{a}t^2\right)\left(1-\frac{c_-}{a}t^2\right)\left(1-\frac{c_+}{a}t^2\right)\right)^{-1} = \\ &= \hat{c}_0\left(1-\frac{c_0}{a}t^2\right)^{-1} + \hat{c}_-\left(1-\frac{c_-}{a}t^2\right)^{-1} + \hat{c}_+\left(1-\frac{c_+}{a}t^2\right)^{-1}, \end{aligned} \tag{A.5}$$

where

$$\hat{c}_0 = \frac{c_0^2}{(c_0-c_-)(c_0-c_+)}, \qquad \hat{c}_- = \frac{c_-^2}{(c_- - c_0)(c_- - c_+)}, \qquad \hat{c}_+ = \frac{c_+^2}{(c_+ - c_0)(c_+ - c_-)}. \tag{A.6}$$

If we take

$$a = \tilde{c}_0, \qquad k^2 = \frac{\tilde{x}_-}{\tilde{x}_+}\frac{1}{a}, \qquad \alpha_0^2 = \frac{c_0}{a}, \qquad \alpha_-^2 = \frac{c_-}{a}, \qquad \alpha_+^2 = \frac{c_+}{a}, \tag{A.7}$$

so that

$$\hat{c}_0 = \frac{\alpha_0^4}{(\alpha_0^2-\alpha_-^2)(\alpha_0^2-\alpha_+^2)}, \qquad \hat{c}_- = \frac{\alpha_-^4}{(\alpha_-^2-\alpha_0^2)(\alpha_-^2-\alpha_+^2)}, \qquad \hat{c}_+ = \frac{\alpha_+^4}{(\alpha_+^2-\alpha_0^2)(\alpha_+^2-\alpha_-^2)}, \tag{A.8}$$

then the integral becomes

$$-t_0 = \frac{E}{2}A\int_0^a \mathrm{d}t\sqrt{\frac{(1-k^2t^2)^5}{1-t^2}}\left(\frac{\hat{c}_0}{(1-\alpha_0^2t^2)}+\frac{\hat{c}_-}{(1-\alpha_-^2t^2)}+\frac{\hat{c}_+}{(1-\alpha_+^2t^2)}\right). \tag{A.9}$$

We now use

$$\sqrt{\frac{1-k^2t^2}{1-t^2}}\frac{1}{(1-\alpha^2t^2)} = \frac{(\alpha^2-k^2)}{\alpha^2}\frac{1}{(1-\alpha^2t^2)\sqrt{(1-t^2)(1-k^2t^2)}}+\frac{k^2}{\alpha^2}\frac{1}{\sqrt{(1-t^2)(1-k^2t^2)}} \tag{A.10}$$

and, noting that

$$\frac{\hat{c}_0}{\alpha_0^2}+\frac{\hat{c}_-}{\alpha_-^2}+\frac{\hat{c}_+}{\alpha_+^2} = 0, \tag{A.11}$$

we have

$$-t_0 = \frac{E}{2}A\int_0^a \mathrm{d}t\frac{(1-k^2t^2)^2}{\sqrt{(1-t^2)(1-k^2t^2)}}\left(I_0+I_-+I_+\right), \tag{A.12}$$

where

$$I_0 = \frac{\alpha_0^2(\alpha_0^2-k^2)}{(\alpha_0^2-\alpha_-^2)(\alpha_0^2-\alpha_+^2)}\ \frac{1}{(1-\alpha_0^2t^2)}, \tag{A.13}$$

$$I_- = \frac{\alpha_-^2(\alpha_-^2-k^2)}{(\alpha_-^2-\alpha_0^2)(\alpha_-^2-\alpha_+^2)}\ \frac{1}{(1-\alpha_-^2t^2)}, \tag{A.14}$$

$$I_+ = \frac{\alpha_+^2(\alpha_+^2-k^2)}{(\alpha_+^2-\alpha_0^2)(\alpha_+^2-\alpha_-^2)}\ \frac{1}{(1-\alpha_+^2t^2)}. \tag{A.15}$$

Each term can now be evaluated [28], to give

$$\begin{aligned}-t_0 = \frac{E}{2}A\Bigg[&\frac{k^6}{\alpha_0^2\alpha_-^2\alpha_+^2}\mathrm{F}(\phi,k)+\frac{(\alpha_0^2-k^2)^3}{\alpha_0^2(\alpha_0^2-\alpha_-^2)(\alpha_0^2-\alpha_+^2)}\Pi(\phi,\alpha_0^2,k)+ \qquad (A.16)\\ &+\frac{(\alpha_-^2-k^2)^3}{\alpha_-^2(\alpha_-^2-\alpha_0^2)(\alpha_-^2-\alpha_+^2)}\Pi(\phi,\alpha_-^2,k)+\frac{(\alpha_+^2-k^2)^3}{\alpha_+^2(\alpha_+^2-\alpha_0^2)(\alpha_+^2-\alpha_-^2)}\Pi(\phi,\alpha_+^2,k)\Bigg],\end{aligned}$$

where $\phi = \sin^{-1} a$. Substituting for the various constants gives the result (3.7) in the text.

References

[1] R. Penrose, in *Batelle rencontres*, C. De Witt and J. Wheeler eds., W.A. Benjamin, 1968.

[2] R.A. Matzner, N. Zamorano and V.D. Sanberg, *Instability of the Cauchy horizon of Reissner-Nordström black holes*, *Phys. Rev.* **D 19** (1979) 2821.

[3] S. Chandrasekhar and J. Hartle, *On crossing the Cauchy horizon of a Reissner-Nordström black-hole*, *Proc. Roy. Soc. Lond.* **A384** (1982) 301.

[4] R. Penrose, *Gravitational collapse: the role of general relativity*, *Nuovo Cim.* **1** (1969) 252 [*Gen. Rel. Grav.* **34** (2002) 1141];
R. Penrose, in *General relativity, an Einstein centenary survey*, S.W. Hawking and W. Israel eds., Cambridge University Press, 1979.

[5] M. Dafermos, *Stability and instability of the reissner-nordstrom cauchy horizon and the problem of uniqueness in general relativity*, gr-qc/0209052; *The interior of charged black holes and the problem of uniqueness in general relativity*, gr-qc/0307013; *Price's law, mass inflation and strong cosmic censorship*, gr-qc/0401121.

[6] V. Balasubramanian and T.S. Levi, *Beyond the veil: inner horizon instability and holography*, *Phys. Rev.* **D 70** (2004) 106005 [hep-th/0405048].

[7] J.M. Maldacena, *The large-N limit of superconformal field theories and supergravity*, *Adv. Theor. Math. Phys.* **2** (1998) 231 [hep-th/9711200];
S.S. Gubser, I.R. Klebanov and A.M. Polyakov, *Gauge theory correlators from non-critical string theory*, *Phys. Lett.* **B 428** (1998) 105 [hep-th/9802109];
E. Witten, *Anti-de Sitter space and holography*, *Adv. Theor. Math. Phys.* **2** (1998) 253 [hep-th/9802150].

[8] E. Witten, *Anti-de Sitter space, thermal phase transition and confinement in gauge theories*, *Adv. Theor. Math. Phys.* **2** (1998) 505 [hep-th/9803131].

[9] T. Hertog, G.T. Horowitz and K. Maeda, *Generic cosmic censorship violation in anti de Sitter space*, *Phys. Rev. Lett.* **92** (2004) 131101 [gr-qc/0307102]; *Negative energy in string theory and cosmic censorship violation*, *Phys. Rev.* **D 69** (2004) 105001 [hep-th/0310054].

[10] G.T. Horowitz and S.F. Ross, *Possible resolution of black hole singularities from large-N gauge theory*, *JHEP* **04** (1998) 015 [hep-th/9803085].

[11] V. Balasubramanian and S.F. Ross, *Holographic particle detection*, *Phys. Rev.* **D 61** (2000) 044007 [hep-th/9906226].

[12] J. Louko, D. Marolf and S.F. Ross, *On geodesic propagators and black hole holography*, *Phys. Rev.* **D 62** (2000) 044041 [hep-th/0002111].

[13] V.E. Hubeny, *Precursors see inside black holes*, *Int. J. Mod. Phys.* **D 12** (2003) 1693 [hep-th/0208047].

[14] J.M. Maldacena, *Eternal black holes in anti-de-sitter*, *JHEP* **04** (2003) 021 [hep-th/0106112].

[15] S. Hemming, E. Keski-Vakkuri and P. Kraus, *Strings in the extended btz spacetime*, *JHEP* **10** (2002) 006 [hep-th/0208003].

[16] P. Kraus, H. Ooguri and S. Shenker, *Inside the horizon with AdS/CFT*, *Phys. Rev.* **D 67** (2003) 124022 [hep-th/0212277].

[17] L. Fidkowski, V. Hubeny, M. Kleban and S. Shenker, *The black hole singularity in AdS/CFT*, *JHEP* **02** (2004) 014 [hep-th/0306170].

[18] T.S. Levi and S.F. Ross, *Holography beyond the horizon and cosmic censorship*, *Phys. Rev.* **D 68** (2003) 044005 [hep-th/0304150].

[19] J. Kaplan, *Extracting data from behind horizons with the AdS/CFT correspondence*, hep-th/0402066.

[20] L. Fidkowski and S. Shenker, *D-brane instability as a large-N phase transition*, hep-th/0406086.

[21] L. Susskind, L. Thorlacius and J. Uglum, *The stretched horizon and black hole complementarity*, *Phys. Rev.* **D 48** (1993) 3743 [hep-th/9306069].

[22] W. Israel, *Thermo field dynamics of black holes*, *Phys. Lett.* **A 57** (1976) 107.

[23] M. Le Bellac, *Thermal field theory*, Cambridge University Press, 1996.

[24] A. Chamblin, R. Emparan, C.V. Johnson and R.C. Myers, *Charged AdS black holes and catastrophic holography*, *Phys. Rev.* **D 60** (1999) 064018 [hep-th/9902170]; *Holography, thermodynamics and fluctuations of charged AdS black holes*, *Phys. Rev.* **D 60** (1999) 104026 [hep-th/9904197].

[25] E. Poisson and W. Israel, *Internal structure of black holes*, *Phys. Rev.* **D 41** (1990) 1796.

[26] D. Brecher, J. He, M. Rozali and P. Saffin, work in progress.

[27] S. Chandrasekhar, *The mathematical theory of black holes*, Oxford University Press, 1985.

[28] P.F. Byrd and M.D. Friedman, *Handbook of elliptic integrals for engineers and physicists*, Springer-Verlag, 1954.

[29] V. Balasubramanian and P. Kraus, *A stress tensor for anti-de Sitter gravity*, *Commun. Math. Phys.* **208** (1999) 413 [hep-th/9902121].

[30] M. Abramowitz and I.A. Stegun, *Handbook of mathematical functions with formulas, graphs, and mathematical tables*, Dover Publications, 1965.

[31] G.W. Gibbons, *Vacuum polarization and the spontaneous loss of charge by black holes*, *Commun. Math. Phys.* **44** (1975) 245.

[32] I.K. Affleck and N.S. Manton, *Monopole pair production in a magnetic field*, *Nucl. Phys.* **B 194** (1982) 38;
I.K. Affleck, O. Alvarez and N.S. Manton, *Pair production at strong coupling in weak external fields*, *Nucl. Phys.* **B 197** (1982) 509.

[33] M. Berkooz, B. Pioline and M. Rozali, *Closed strings in misner space: cosmological production of winding strings*, *JCAP* **08** (2004) 004 [hep-th/0405126].

[34] T. Friedmann and H. Verlinde, *Schwinger pair creation of Kaluza-Klein particles: pair creation without tunneling*, *Phys. Rev.* **D 71** (2005) 064018 [hep-th/0212163].

[35] M. Berkooz, B. Craps, D. Kutasov and G. Rajesh, *Comments on cosmological singularities in string theory*, *JHEP* **03** (2003) 031 [hep-th/0212215].

[36] W.B. Bonnor and P. C. Vaidya, *Spherically symmetric radiation of charge in Einstein-Maxwell theory*, *Gen. Rel. Grav.* **1** (1970) 127;
B.T. Sullivan and W. Israel, *The third law of black hole mechanics: what is it?*, *Phys. Lett.* **A 79** (1980) 371.

[37] J.S.F. Chan and R.B. Mann, *Scalar wave fall off in asymptotically anti-de Sitter backgrounds*, *Phys. Rev.* **D 55** (1997) 7546 [gr-qc/9612026].

[38] C. Barrabés and W. Israel, *Thin shells in general relativity and cosmology: the lightlike limit*, *Phys. Rev.* **D 43** (1991) 1129.